CEVANS/057/FR-8901

(2)

Final Report

DEVELOPMENT AND EVALUATION OF AN INSTRUMENT FOR RAPID ELECTROREFLECTANCE OF SEMICONDUCTOR MATERIALS

AD-A211 690

Prepared by:

Michael H. Herman, Ph.D.

CHARLES EVANS & ASSOCIATES
301 Chesapeake Drive
Redwood City, CA 94063
(415) 369-4567

Reporting Period: February 1, 1988 - April 30, 1989

Sponsored by:

Defense Advanced Research Projects Agency (DOD)
1400 Wilson Blvd
Arlington, VA 22209-2308

ARPA Order No. 5325

Issued by Office of Naval Research Under
Contract No. N00014-88-C-0221

DTIC
ELECTE
AUG 2 4 1989
S D
D

Principal Investigator:

Michael H. Herman

Effective Date of Contract: February 1, 1988
Contract Expiration Date: April 30, 1989

June 30, 1989

The views and conclusions contained in this document are those of the authors and should not be interpreted as necessarily representing the official policies, either express or implied, of the Defense Advanced Research Projects Agency or the U.S. Government.

APPROVED FOR PUBLIC RELEASE
DISTRIBUTION UNLIMITED

89 8 23 455

UNCLASSIFIED
SECURITY CLASSIFICATION OF THIS PAGE

REPORT DOCUMENTATION PAGE

Form Approved
OMB No 0704-0188
Exp Date Jun 30, 1986

1a REPORT SECURITY CLASSIFICATION UNCLASSIFIED	1b RESTRICTIVE MARKINGS
2a SECURITY CLASSIFICATION AUTHORITY —	3 DISTRIBUTION/AVAILABILITY OF REPORT APPROVED FOR PUBLIC RELEASE DISTRIBUTION UNLIMITED
2b DECLASSIFICATION/DOWNGRADING SCHEDULE —	
4 PERFORMING ORGANIZATION REPORT NUMBER(S) CEVANS/057/FR-8901	5 MONITORING ORGANIZATION REPORT NUMBER(S)
6a NAME OF PERFORMING ORGANIZATION CHARLES EVANS & ASSOCIATES 6b OFFICE SYMBOL (If applicable) ST252	7a NAME OF MONITORING ORGANIZATION Office of Naval Research
6c ADDRESS (City, State, and ZIP Code) 301 Chesapeake Drive Redwood City, CA 94063	7b ADDRESS (City, State, and ZIP Code) 800 N. Quincy Street Arlington, VA 22217-5000
8a NAME OF FUNDING/SPONSORING ORGANIZATION DARPA 8b OFFICE SYMBOL (If applicable)	9 PROCUREMENT INSTRUMENT IDENTIFICATION NUMBER N00014-88-C-0221
8c ADDRESS (City, State, and ZIP Code) 1400 Wilson Blvd Arlington, VA 22209	10 SOURCE OF FUNDING NUMBERS PROGRAM ELEMENT NO / PROJECT NO / TASK NO / WORK UNIT ACCESSION NO

11 TITLE (Include Security Classification) UNCLASSIFIED - DEVELOPMENT AND EVALUATION OF AN INSTRUMENT FOR RAPID ELECTROREFLECTANCE OF SEMICONDUCTOR MATERIALS

12 PERSONAL AUTHOR(S)
Michael H. Herman

13a TYPE OF REPORT	13b TIME COVERED	14 DATE OF REPORT (Year, Month, Day)	15 PAGE COUNT
Final Technical	FROM 01Feb88 TO 30Apr89	June 30, 1989	69

16 SUPPLEMENTARY NOTATION

17 COSATI CODES			18 SUBJECT TERMS (Continue on reverse if necessary and identify by block number)
FIELD	GROUP	SUB-GROUP	

19 ABSTRACT (Continue on reverse if necessary and identify by block number)

The applications of Electron Beam Electroreflectance (EBER) to $Hg_{1-x}Cd_xTe$ (MCT) and other semiconductor systems are described. Temperature dependences of the E_1 optical gap of MCT are in agreement with the results of other researchers. For an epitaxial sample, $\partial E_1/\partial T$ of -(6.7 to 8.2)x10^{-4} eV/K has been obtained. This value is consistent with that determined by Berlouis (-6.6 ± 0.5) x 10^{-4} eV/K). As did Berlouis, we find a larger thermal coefficient for epitaxial MCT on CdTe than for bulk MCT. We have also measured the $E_1+\Delta_1$ band gap to be nearly 0.63 eV above the E_1 transition energy. Our data suggests that Δ_1 is 0.625 ± 0.012, and has a temperature dependence between 5 x 10^{-5} eV/K and 2 x 10^{-4} eV/K. The $E_1+\Delta_1$ band gap has a dependence of about -5 x 10^{-4} eV/K.

MCT is more sensitive to electron beam current intensity than other materials due to its relatively poor thermal conductivity. The lineshape observed at 10^{-3} A/cm^2 appears to be from thermoreflectance (TR), based upon calculations and detailed experimental studies.

20 DISTRIBUTION/AVAILABILITY OF ABSTRACT ☐ UNCLASSIFIED/UNLIMITED ☐ SAME AS RPT ☐ DTIC USERS	21 ABSTRACT SECURITY CLASSIFICATION UNCLASSIFIED
22a NAME OF RESPONSIBLE INDIVIDUAL GT. Winn	22b TELEPHONE (Include Area Code) / 22c OFFICE SYMBOL

DD FORM 1473, 84 MAR — 83 APR edition may be used until exhausted. All other editions are obsolete

SECURITY CLASSIFICATION OF THIS PAGE

UNCLASSIFIED

Therefore, EBER determinations of the temperature dependence of the E_1 and $E_1+\Delta_1$ band gap energies demonstrate a large variance.

Further, we have collaborated with other researchers on EBER evaluation of MCT growth and dry-etch processes. We have worked with Stanford University students on evaluation of VPE grown MCT on CdTe substrates, compositional variations from dry etching of MCT for the Army Night Vision Laboratories and Plasmaquest Corporation.

Additionally, we have extended EBER studies to other technologically important crystal systems related to MCT. We have found correlations between the EBER measurements of CdTe samples and surface preparation methods. In the case of GaAs and related compounds, our results have shown promise in the analysis of epitaxial films and heterostructures, which are briefly described.

Accesion For
NTIS CRA&I ☑
DTIC TAB ☐
Unannounced ☐
Justification
By
Distribution /
Availability Codes
Dist | Avail and / or Special
A-1

SUMMARY

The applications of electron beam electroreflectance (EBER) to $Hg_{1-x}Cd_xTe$ (MCT) and other semiconductor systems are described. Temperature dependences of the E_1 optical gap of MCT are in agreement with the results of other researchers. For an epitaxial sample, $\partial E_1/\partial T$ of -(6.7 to 8.2) x 10^{-4} eV/K has been obtained. This value is consistent with that determined by Berlouis. (-6.6 (± 0.5) x 10^{-4} eV/K). As did Berlouis, we find a larger thermal coefficient for epitaxial MCT on CdTe than for bulk MCT. We have also measured the $E_1+\Delta_1$ band gap to be nearly 0.63 eV above the E_1 transition energy. Our data suggests that Δ_1 is 0.625 (± 0.012), and has a temperature dependence between 5 x 10^{-5} eV/K and 2 x 10^{-4} eV/K. The $E_1+\Delta_1$ band gap has a dependence of about -5 x 10^{-4} eV/K.

MCT is more sensitive to electron beam current intensity than other materials due to its relatively poor thermal conductivity. The lineshape observed at 10^{-3} A/cm^2 appears to be from thermoreflectance (TR), based upon calculations and detailed experimental studies. Therefore, EBER determinations of the temperature dependence of the E_1 and $E_1+\Delta_1$ band gap energies demonstrate a large variance.

Further, we have collaborated with other researchers on EBER evaluation of MCT growth and dry-etch processes. We have worked with Stanford University students on evaluation of VPE grown MCT on CdTe substrates and compositional variations from dry etching of MCT for the Army Night Vision Laboratories and Plasmaquest Corporation.

Additionally, we have extended EBER studies to other technologically important crystal systems related to MCT. We have found correlations between the EBER measurements of CdTe samples and surface preparation methods. In the case of GaAs and related compounds, our results have shown promise in the analysis of epitaxial films and heterostructures, which are briefly described.

ACKNOWLEDGEMENTS

Many groups were helpful in providing useful samples and information. Dr. Paul Armitharaj of the Army Night Vision Laboratories provided reprints of several of his pertinent research papers on MCT. Material for study was also provided to us by John Spencer of Plasmaquest, Inc, and by Dr. Jack Dinan of the Army Night Vision Laboratories. Dr. Paul Koppel of McDonnell Douglas also allowed us to study many samples of various carrier types and conductivity. Dr. Bill Micklethwaite of Cominco Corp. kindly provided us with the published data on the thermal properties of MCT. Dr. Joe Schmidt of Honeywell Corp. also provided us with information about the measurements of physical properties of MCT. Stanford students Seung Bae Lee and Jane Farthing of Professor Stevenson's group also allowed us to examine several of their iso-VPE grown epitaxial MCT samples.

During the course of this research, we benefitted from the collaboration of many individuals. Dr. S. E. Buttrill, who designed and built the EBER research instrument, conducted the initial investigations of the temperature dependence of the MCT E_1 and $E_1+\Delta_1$ band gaps. Lee Francke designed and built the detector electronics and software, and also ran many of the MCT samples during this study. Ian Ward carefully conducted many of the experiments of low electron beam current and frequency dependence, providing much of the evidence for the TR mechanism, and showing that ER signals could be obtained from MCT. We were able to study the PzR mechanism from the sample kindly provided to us by Glen Carey, a student of Professor Spicer, at Stanford University. Professor Paul Raccah of the University of Illinois at Chicago consulted strongly during our research on MCT, providing alternative suggestions about potential modulation mechanisms, and fitting approaches for their analysis. Dr. David Reed provided helpful feedback in regards to the TR mechanism and careful review of the manuscript. Lastly, we thank D. Rocha and S. Kerr for the final preparation of the manuscript.

CONTENTS

Page

I. INTRODUCTION 1

II. RESULTS 1

1. Studies of the effects of electron beam current on non-destructive EBER measurements. 1

2. Tests of the mechanism of first derivative lineshapes for MCT. 4

3. Comparison of experimental conditions and theoretical fit parameters on estimation of band gaps and broadening parameters. 13

4. Studies of EBER detection of electron beam effects on the MCT surface and calculation of thermal effects. 17

5. Investigations of the temperature dependence of the E_1 band gap of MCT by EBER. 28

6. Investigations of the surface treatments of bulk CdTe at the E_0 band gap by EBER. 33

7. Studies of GaAs and related compounds. 33

III. CONCLUSION 35

FIGURES

Page

FIGURE 1. The correlation between E_1 and x value, at room temperature (taken to be 300 K). From P. M. Raccah and U. Lee, J. Vac. Sci & Technol. A1(3), 1587-1592, 1983. Their expression: $E_1(x) = 2.135 + 0.600x + (0.640\ (\pm 0.05))x^2$. 2

CONTENTS

Page

FIGURE 2. Illustration of ER and TR as third and first derivatives of ϵ, respectively. The theoretical lineshape predicted for first, second, and third derivatives of ϵ_2 are shown for a parabolic critical point. The ϵ_2 function is the imaginary part of the dielectric function ϵ, and corresponds to absorption. The actual high electron beam current density EBER data for MCT closely resembles the "Thermo/Piezo-Reflectance" curve shown, but inverted in phase. 3

3. Representative EBER spectrum of MCT at 159 K. The completely first derivative lineshape fits the experimental data reasonably well, as shown. 5

4. The EBER spectrum of [110]-oriented and [111]-oriented MCT. Note that the same first derivative lineshape is experimentally observed for both. 6

5. The EBER spectra of expitaxial MCT on CdTe, obtained at two different measurement frequencies. Figure 5a shows the broad features characteristic of first derivative spectra at 260 Hz. Figure 5b shows the derivative spectra at 630 Hz. Both spectra were obtained at the same sample position beam current (12 μA) and temperature (97 K) 8

6. The EBER spectrum of sample #52 at low current density. Note that the theoretical fit using a third derivative is adequate to represent the experimental features. 10

7. The EBER spectrum of sample #52 at intermediate current density. A theoretical fit requires both a third derivative and a first derivative component to represent the experimental data. 11

8. The EBER spectrum of sample #52 at high current density. Note that the theoretical fit using a first derivative is adequate to represent the experimental features. 12

9. High electron beam current (40 μA) MCT study showing the temperature dependence of the E_1 band gap. The back of the sample was mounted to a copper holder with silver paint. The data is fit to a linear E_1 temperature dependence ($\partial E_1/\partial T$) of -4.582 ($\pm$0.062) x 10^{-4} eV/K. 19

10. Deviations from linearity in Figure 6. 20

CONTENTS

Page

FIGURE 11. The MCT study showing changes in 90 K E_1 energies after EBER analysis at 190 K and 210 K under high electron beam current (40 μA) conditions. The data suggests that Hg is lost from the surface, resulting in a net increase in Cd and an increase in E_1 band gap energy..... 21

12. The EBER study of sample 56-1 (MCT epi on CdTe) showing a sequence of E_1 band gap measurements (listed in Table 4). The figure shows that the 90 K transition increases significantly in point #15, which followed the 400 K measurement. The temperature dependence from these measurements, also listed in Table 4, is $\partial E_1/\partial T = -3.59$ (± 0.25) x 10^{-4} eV/K. 22

13. The EBER study of sample 56-1 (MCT epi on CdTe) showing both the E_1 and the $E_1+\Delta_1$ transition energies. $\partial\Delta_1/\partial T$ is measured for this sample at only 4.23 (± 2.8) x 10^{-5} eV/K, demonstrating that the two transitions have essentially identical temperature dependence. 23

14. Results of EBER analysis of a sample of MCT under low electron beam current density conditions. We observe that the E_1 energy measured at 95 K changed by a negligible degree after cycling even to 300 K under electron beam irradiation, in ultra-high vacuum. However, following measurements at 350 and 400 K, there was an increase in the E_1 transition energy corresponding to Hg loss from the surface. 26

15. Original sample holder with single Cu-Be clip. 30

16. Revised sample holder with Cu-Be surface gasket. 31

17. The EBER spectra of three samples of [111]-oriented CdTe at 300 K. The three CdTe surfaces had (a) a mechanical 0.3 μm diamond polish, (b) an alternative "diamond turned" surface and (c), a combination of mechanical and chemical polish. . 34

TABLES

Page

TABLE 1. Effects of EBER measurement frequency on MCT data using GFF model. 9

CONTENTS

			Page
TABLE	2.	Results of fitting MCT data to GFF model. Comparison of third derivative to GFF (1+2+3 D) fits.	14
	3A.	Results sequential study of E_1, $E_1+\Delta_1$ and Δ_1 band gaps	24
	3B.	Linear regression analysis: $E(T) = A + BT$ (excluding File 11).	24
	4.	Peak surface temperature from electron beam heating.	27
	5.	Temperature dependence of E_1 band gap on MCT mount	29
	6.	Temperature dependence of MCT $E_1+\Delta_1$ and Δ_1 band gaps. (All from epitaxial sample 52 with Cu gasket mount.)	33

PUBLICATIONS AND PRESENTATIONS 37

REFERENCES 38

APPENDIX 40

I. INTRODUCTION

The primary objective of this research has been the accurate determination of the temperature dependence of the E_1 band gap of $Hg_{1-x}Cd_xTe$ (MCT). We have tested as wide a range of x-values as we could obtain, and made measurements between 90 K and 400 K--the widest temperature range yet studied by electroreflectance for this materials system. We also planned to obtain the $E_1+\Delta_1$ energy gap information, so that the difference Δ_1 could be evaluated as a function of composition.

Originally, we expected to measure the Cd fraction by independent methods (electron microprobe, IR transmission, X-ray diffraction, thermogravometric). However, to avoid the difficulties and uncertainties associated with independent measurements of the Cd fraction, we chose instead to use the established room temperature optical E_1 correlation to x-value determinations,[1] shown in Figure 1, for evaluating the MCT composition. This allowed us to use the EBER measured E_1 band gap at 300 K to determine the composition of each sample <u>at the point under optical examination</u>. Therefore, samples which may have contained variations in Cd content across the surface remained valid for measurements by EBER for this research. Furthermore, should a better expression of $E_1(x)$ become available in the future, our temperature dependence data will remain valid.

II. RESULTS

1. STUDIES OF THE EFFECTS OF ELECTRON BEAM CURRENT ON NONDESTRUCTIVE EBER MEASUREMENTS.

For the measurement of band gap energies by modulation spectroscopies, one generally desires as narrow a lineshape as possible, so that accurate estimations of peak energies may be made. Presently, this issue is less critical due to the availability of rapid least-squares fitting algorithms and effective theoretical models for the critical points of the solid. Still, present theoretical models assume band parabolicity in the vicinity of the critical point energy, and this assumption is known to break down at energies far from the critical point. It is therefore considered most favorable if the modulated reflectance signals are narrow in energy.

All other experimental variables held constant, electric field modulation of the sample (electroreflectance or ER), provides more narrow lines than thermoreflectance (TR) arising from temperature modulation. This is due to the higher derivative of the dielectric function ϵ which is obtained experimentally from ER modulation.[2] Specifically, ER gives a third derivative of ϵ, rather than the first derivative from TR.[3] These cases are demonstrated in Figure 2, which shows the derivatives of a parabolic critical point. More importantly, the ER mechanism does not affect the sample temperature nor the (temperature-dependent) band gap energies, whereas the TR mechanism affects both. Experimentally, first derivative TR-like lineshapes were observed from MCT in the earliest investigations by EBER.[4] It was therefore important for us to examine the potential for TR effects in EBER measurements of MCT.

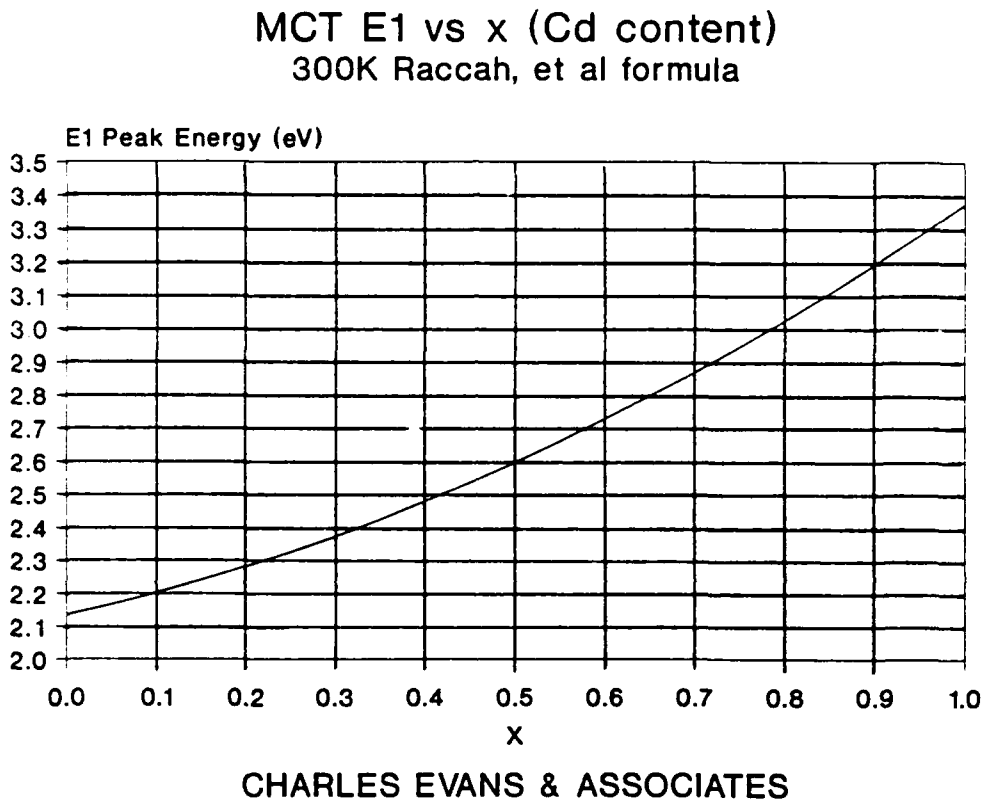

Figure 1. The correlation between E_1 and x value, at room temperature (taken to be 300 K). From P. M. Raccah and U. Lee, J. Vac. Sci & Technol. A1(3), 1587-1592, 1983. Their expression: $E_1(x) = 2.135 + 0.600x + (0.640\ (\pm 0.05))x^2$.

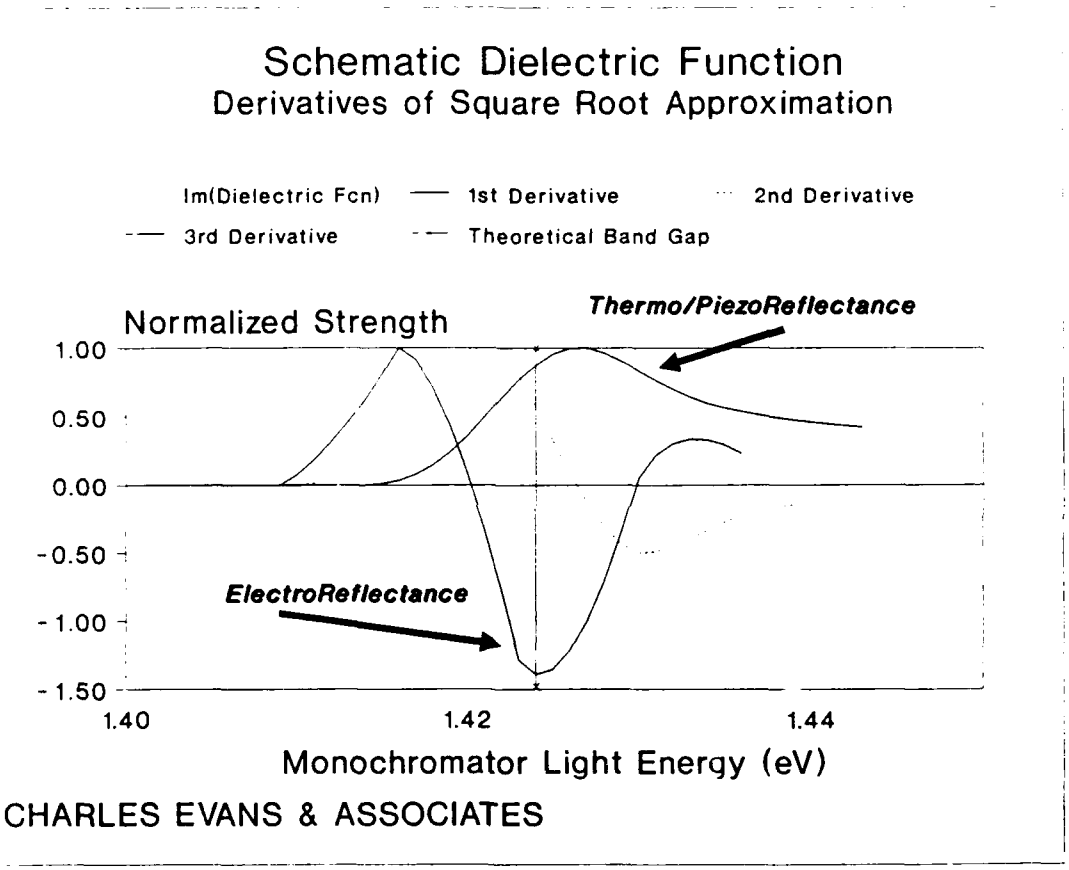

Figure 2. Illustration of ER and TR as third and first derivatives of ϵ, respectively. The theoretical lineshape predicted for first, second, and third derivatives of ϵ_2 are shown for a parabolic critical point. The ϵ_2 function is the imaginary part of the dielectric function ϵ, and corresponds to absorption. The actual high electron beam current density EBER data for MCT closely resembles the "Thermo/Piezo-Reflectance" curve shown, but inverted in phase.

2. TESTS OF THE MECHANISM OF FIRST DERIVATIVE LINESHAPES FOR MCT

a. Evaluation of piezoreflectance induced by electric fields in EBER.

The observations of first derivative signals from our previous EBER experiments were incommensurate with electroreflectance (ER), and suggested that alternative modulation mechanisms were responsible. Earlier work had demonstrated primarily first derivative EBER signals from MCT samples at low electron beam current densities, even though third derivative signals were observed on the same samples by electrolyte ER (EER). A typical spectrum of both the E_1 and $E_1+\Delta_1$ energy gaps appears in Figure 3, along with the first derivative theoretical fits. These first derivative signals at first suggested that thermoreflectance (TR) resulted from the electron beam heating of the surface. However, a calculation led us to expect that this effect should be inconsequential.[5]

b. Evaluation of piezoelectrically induced modulated reflectance of MCT.

Other mechanisms were suggested and evaluated. It was hypothesized that the first derivative shape may be due to either a band-filling mechanism,[6] or piezoelectrically induced piezoreflectance (PzR).[7] The PzR was evaluated experimentally by comparing the lineshape at two different crystal orientations. The PzR can be induced by surface charge if the crystallographic direction of the sample permits electrostriction to occur. Electric fields may produce PzR at a polar face only; in the case of MCT, the [110] face is non-polar, prohibiting field-induced PzR.

To test the PzR mechanism, we obtained a crystal of [110]-oriented MCT from Glen Carey, a student of Professor Spicer, at Stanford University. The sample was cleaved at our laboratory, and was tested under standard conditions. The results appear in Figure 4. As this figure shows, we obtained similar first derivative results on the [110] sample as for our typical [111]-oriented samples. Differences in signal intensity between the [111] and [110] samples do not conclusively show that PzR is completely absent--to do so requires further studies with identically prepared samples, surfaces and experimental conditions. However, we conclude that field-induced PzR is improbable as the major cause of the first derivative lineshape obtained with EBER of MCT.

c. Evaluation of the band-filling mechanism in modulated reflectance of MCT.

The band-filling mechanism has also been suggested as an explanation of the EBER lineshape of MCT. The band-filling mechanism has been proposed to account for changes in E_0 band gap energy which occur when the carrier density exceeds the effective density of states of the conduction band (in n-type materials) or valence band (in p-type materials). This is, in effect, taking account of the Burstein shift mechanism. In MCT, these effective densities of states are quite small, owing to the very small effective masses of the carriers, so that degeneracy conditions are expected to be dominant. However, the populations of the higher-lying E_1 and $E_1+\Delta_1$ band gaps must be small and non-degenerate, owing to their large energy spacing from the Fermi level in

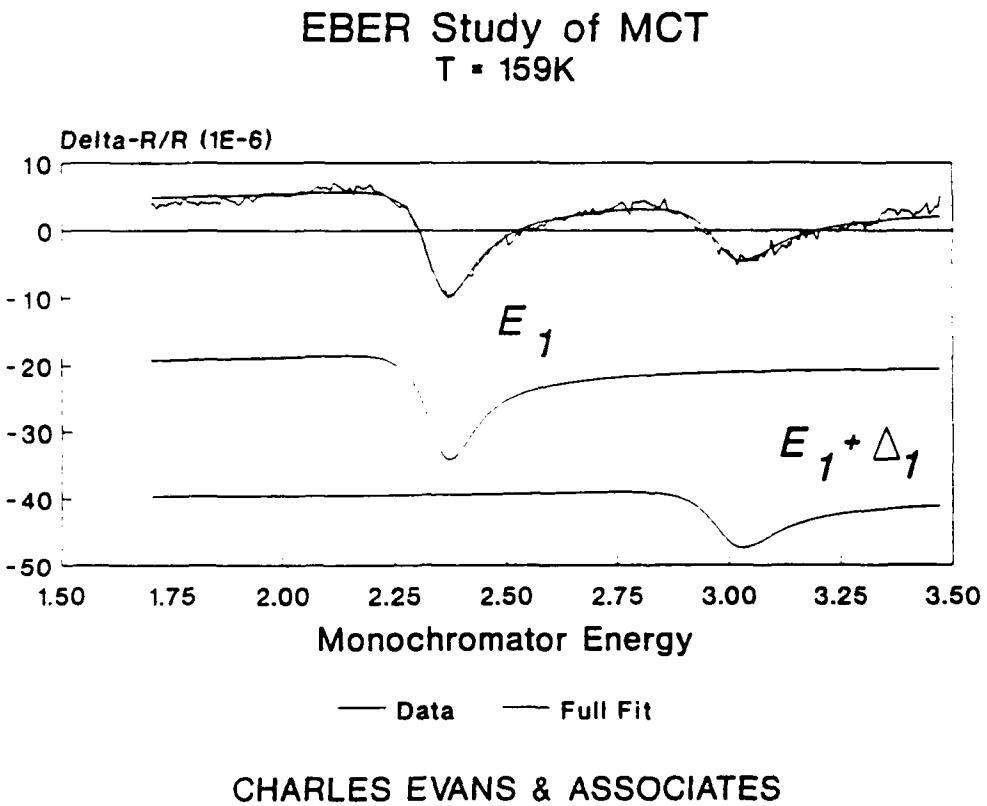

Figure 3. Representative EBER spectrum of MCT at 159 K. The completely first derivative lineshape fits the experimental data reasonably well, as shown.

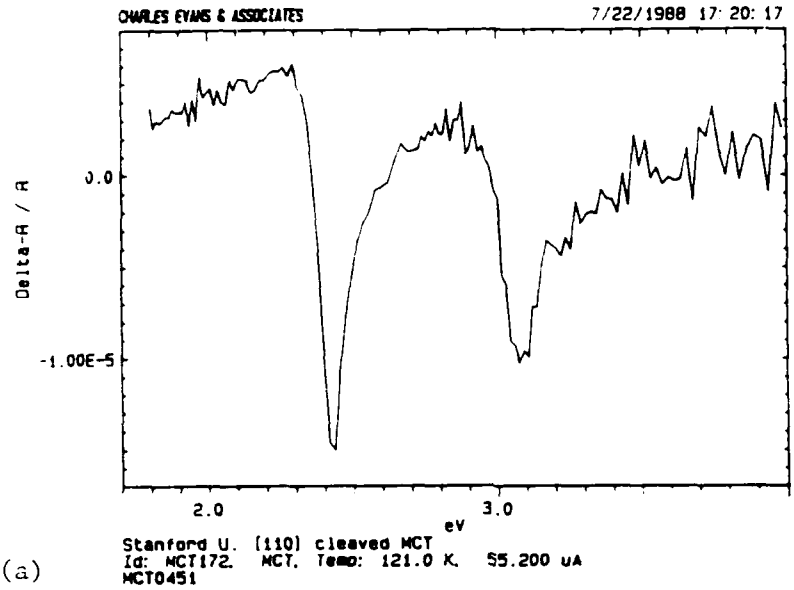

(a)

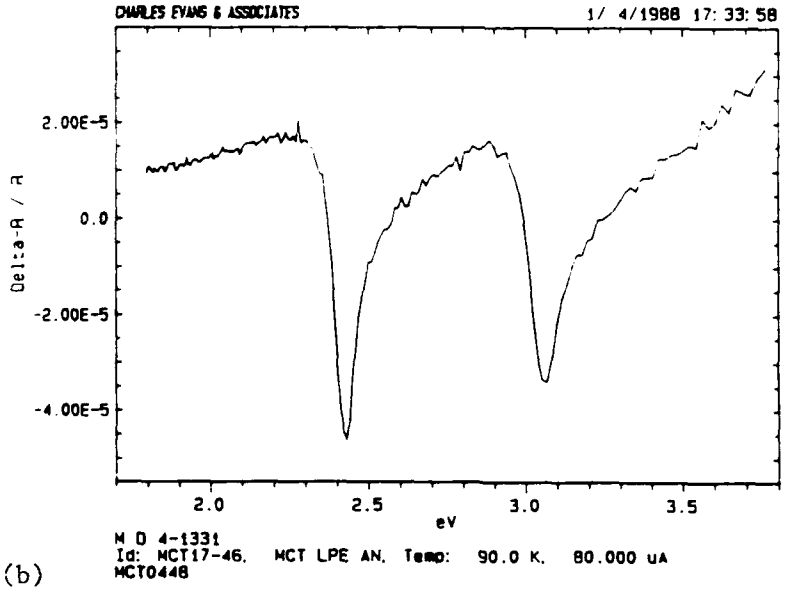

(b)

Figure 4. EBER spectrum of (a) [110]-oriented and (b) [111]-oriented MCT. Note that the same first derivative lineshape is experimentally observed for both.

the MCT. Therefore, we do not expect that band-filling at E_0 to play a major role in the higher energy band gaps of MCT.

However, a refinement of the band-filling argument was proposed by Professor Raccah of the University of Illinois at Chicago.[8] Dr. Raccah suggested that the degeneracies near E_0 may affect the higher energy band gaps regardless, due to free carrier interactions within the crystal. If that argument is correct, then the band-filling mechanism should be present in MCT under any conditions, as the material can be considered degenerate for low x values. Therefore, we should observe a first derivative lineshape at all electron beam currents in EBER measurements and at all frequencies of measurement. We tested this hypothesis experimentally.

We have compared the band-filling and TR mechanisms, using the measurement frequency. The band-filling takes place very quickly on the time scale of the measurements (1/200 second, or 5 milliseconds typically). However, the heat delivered per cycle should be proportional to the time that the electron beam irradiates the surface per cycle (see the calculation in section I.4). Therefore, by increasing the electron beam modulation frequency, band-filling effects should be unaffected, but TR effects should be reduced. We find experimentally that the first derivative component of the lineshape is diminished as the measurement frequency is raised, supporting the TR mechanism.

The data in Figure 5 shows the results of two sequential EBER measurements on the same MCT sample. Both spectra were acquired at identical stage temperatures (96 K) and electron beam currents (12 μA). At 260 Hz, in Figure 5a, we observe the characteristic first derivative lineshape. In contrast, at 630 Hz, in Figure 5b, we observe an additional rise of the leading edge of each peak, indicating a third derivative component. Table 1 below shows the comparison of the fitting parameters for the two cases. The last column shows the ratio of third derivative to first derivative amplitudes, and is a measure of the ER/TR contributions. At the higher frequency, the ratio has increased by about 40%. These results are consistent with those of Broser *et al.* in cathodoreflectance measurements on germanium.[9] We observe that the differences in energy estimates are statistically insignificant, given the estimated errors.

d. Evaluation of the thermoreflectance mechanism in EBER studies of MCT.

To further distinguish between the possible origins of the first derivative lineshape, we investigated the effects of electron beam current. It was hypothesized that observation of a third derivative lineshape at low electron beam current densities would also tend to discount the band-filling mechanism, and support instead TR as the most likely cause of the first derivative lineshapes at high electron beam current densities. Therefore, we investigated the detection of very weak signals using low (~1 μA) electron beam currents. If the same first derivative lineshapes were always obtained, it would support the band-filling mechanism, and negate the TR mechanism. Conversely, if a clear, third derivative lineshape were obtained at low current, it would support the TR mechanism at high electron beam currents.

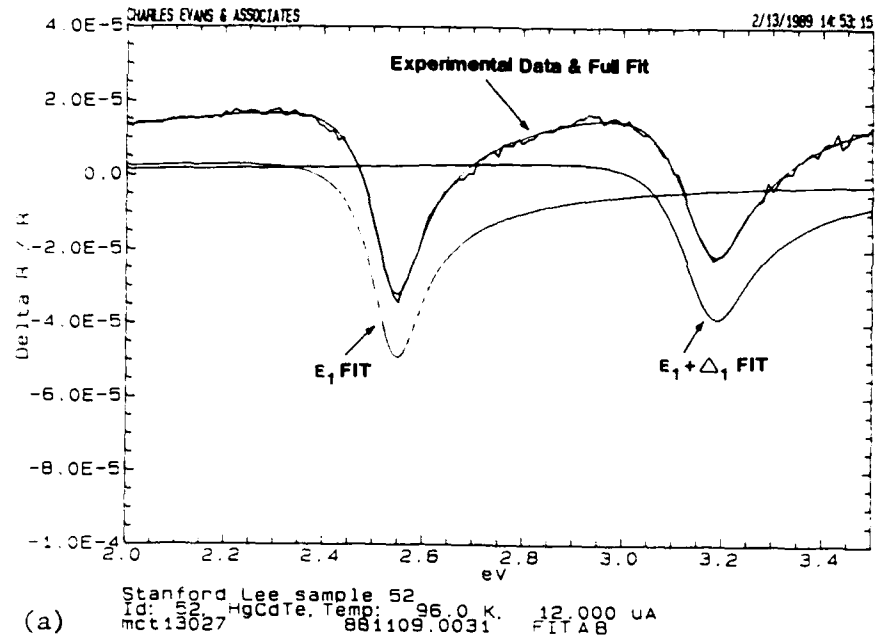

(a)

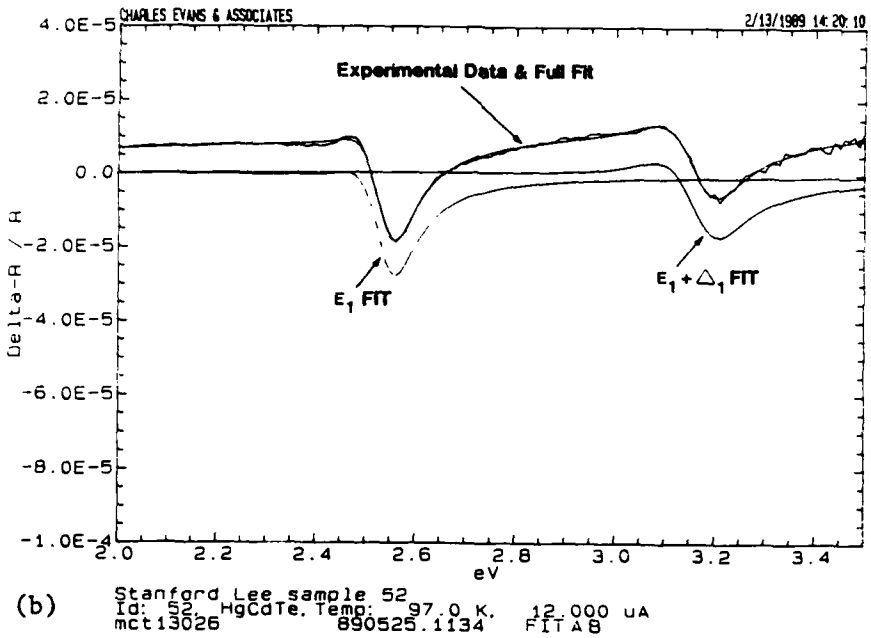

(b)

Figure 5. EBER spectra of epitaxial MCT on CdTe, obtained at two different measurement frequencies. Figure 5a shows the broad features characteristic of first derivative spectra at 260 Hz. Figure 5b shows the sharper features characteristic of third derivative spectra at 630 Hz. Both spectra were obtained at the same sample position beam current (12 μA), and temperature (97 K).

Table 1. Effects of EBER measurement frequency on MCT data using GFF model.

Frequency (Hz)	E_1 (eV)	$E_1+\Delta_1$ (eV)	Γ_{E1} (meV)	$\Gamma_{E1+\Delta1}$ (meV)	A_3/A_1 for E_1[a] (10^{-3})
		Comparison of GFF (1+2+3 D) Fits			
260	2.537 {0.003}	3.172 {0.011}	91.3 {7.5}	97.6 {6.6}	2.52
630	2.541 {0.003}	3.174 {0.004}	76.9 {4.6}	112.3 {5.9}	3.48
ave:	2.539	3.173	84.1	104.9	
std. meas.	0.003	0.002	10.2	10.4	
std. joint	0.004	0.012	8.8	8.9	

Notes:
1. Dimensionalities = 2 for both E_1 and $E_1+\Delta_1$.
2. Standard error in brackets ({}).

[a]A_3/A_1 is the ratio of third derivative to first derivative component

The results supported the TR mechanism. We found that by sufficiently careful data acquisition, we could obtain third derivative EBER spectra of MCT with very low electron beam current densities. The fact that lineshapes characteristic of electroreflectance could be obtained with very low electron beam current densities suggested that ER is possible for MCT in this mode. The results of these experiments appear in Figures 6 through 8. In Figure 6, we show that very low electron beam current (0.6 μA) gives an EBER signal which can be accurately fitted to a pure third derivative lineshape. Figure 7 shows the same sample, taken subsequently with a higher electron beam current of 8 μA. The spectrum has changed in quite an obvious manner, and the theoretical fitting of the data, attached in Table 2, shows that although the third derivative is still present, the first derivative component of the spectrum has dramatically increased in amplitude by almost 100 times. Figure 8 shows the same sample, taken subsequently with an electron beam current of 11 μA, but at more focussed conditions corresponding to a higher electron beam current density. In that case, the first derivative component of the spectrum has dramatically increased. These experiments have been repeated on several samples.

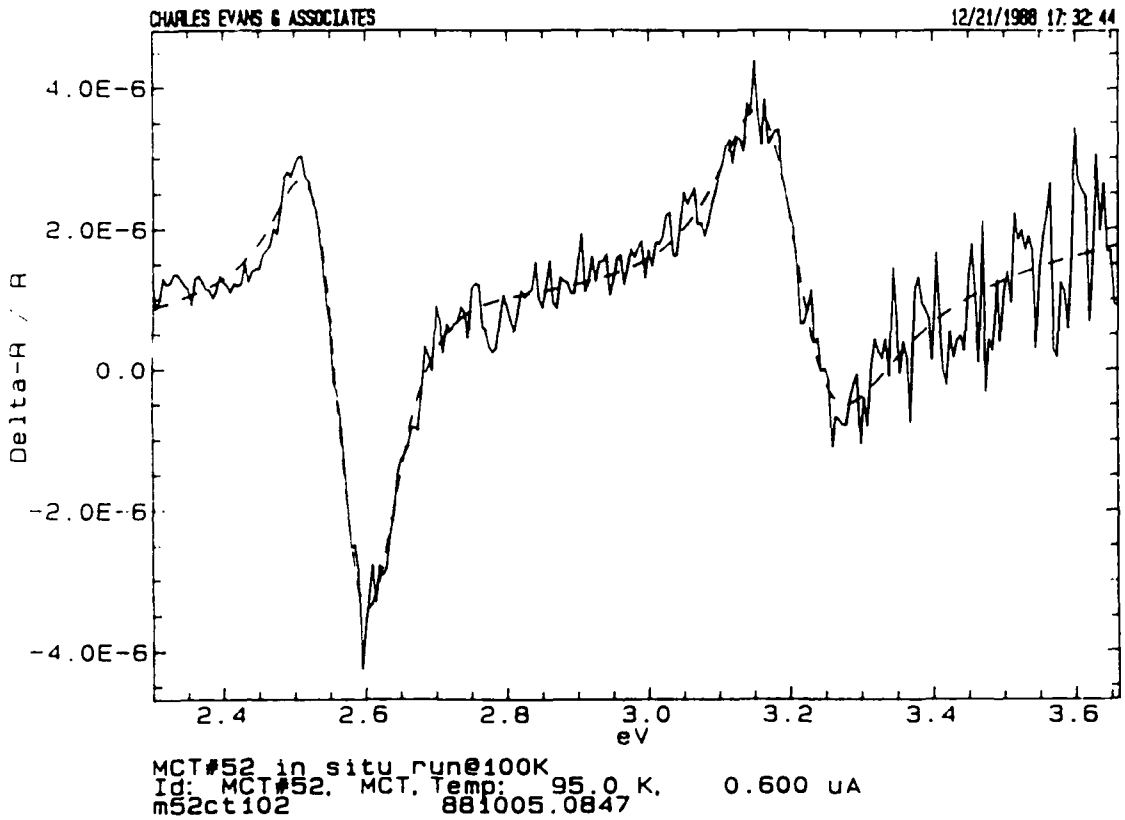

Figure 6. The EBER spectrum of sample #52 at low current density. Note that the theoretical fit using a third derivative is adequate to represent the experimental features.

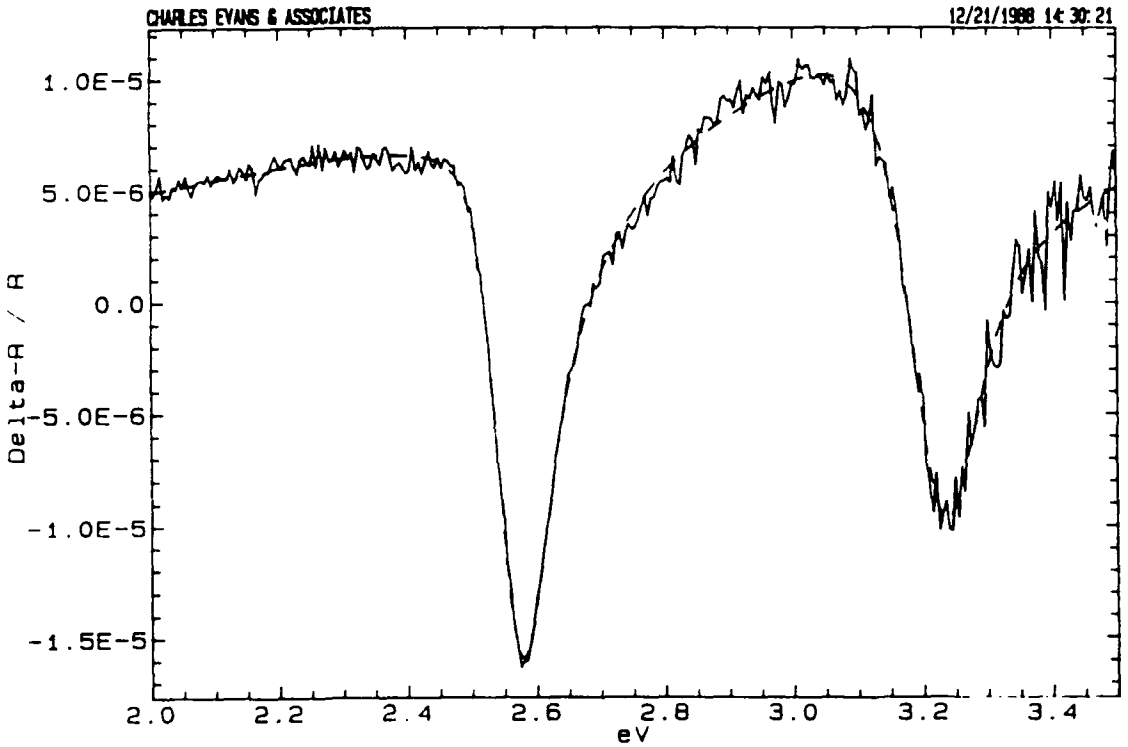

Figure 7. The EBER spectrum of sample #52 at intermediate current density of 8 μA. A theoretical fit requires both a third derivative and a first derivative component to represent the experimental data.

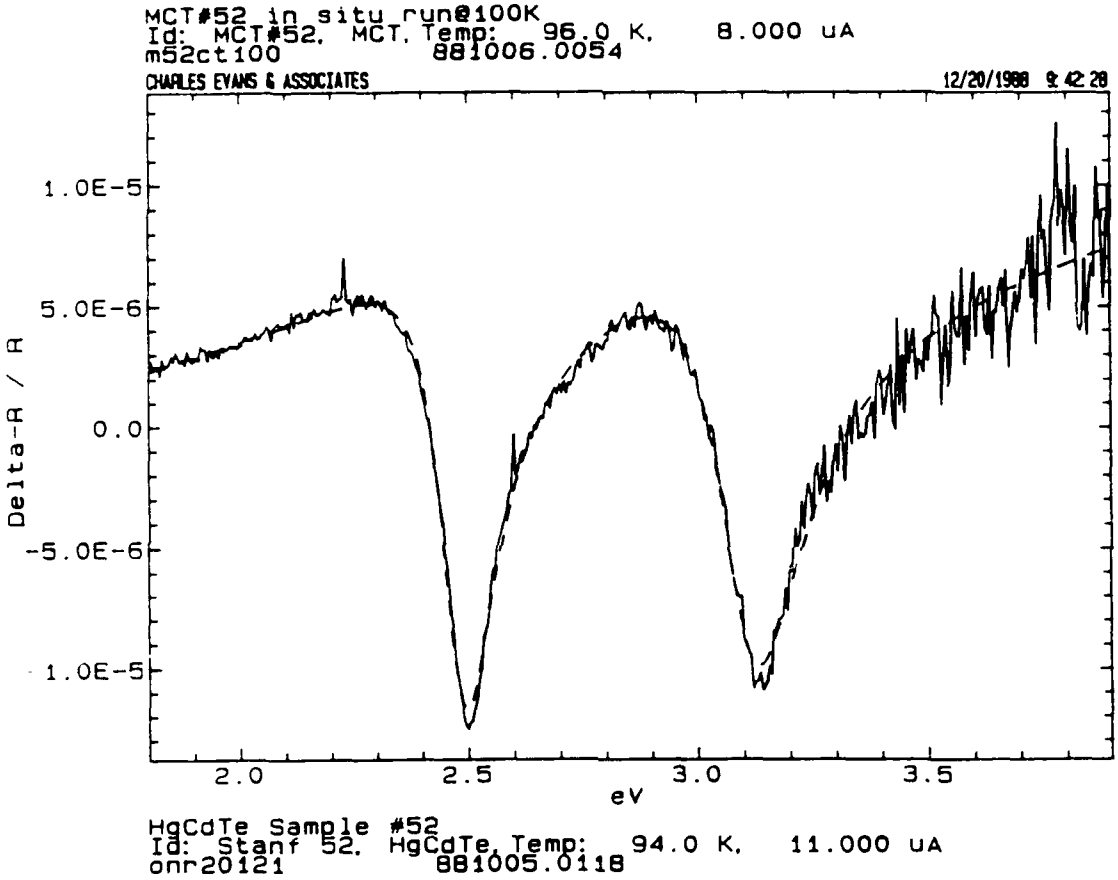

Figure 8. The EBER spectrum of sample #52 at high current density. Note that the theoretical fit using a first derivative is adequate to represent the experimental features.

3. COMPARISON OF EXPERIMENTAL CONDITIONS AND THEORETICAL FIT PARAMETERS ON ESTIMATION OF BAND GAPS AND BROADENING PARAMETERS.

To achieve our research goal required numerical fitting of our experimental EBER data to established models for optical transitions. In the case of MCT, we consistently used a two-dimensional Lorentzian lineshape to model the transitions E_1 and $E_1+\Delta_1$. As described above (in section II.1), the physical modulation mechanism affects the theoretical derivative of the dielectric function appropriate for fitting. For the TR mechanism, the first derivative is appropriate; for ER, the third derivative is correct. In addition, Garland and Raccah[10] have suggested that the second derivative may provide a contribution proportional to inhomogeneous broadening from defects in the solid. The resulting "Generalized Functional Form" (GFF) of Garland and Raccah may contain all three derivative components.

a. Comparison of low and high current density results.

We now compare the estimates of band gaps (E_1, $E_1+\Delta_1$) and broadening parameters (Γ_{E1}, $\Gamma_{E1+\Delta 1}$) obtained from fitting the low, medium, and high current density spectra using the Generalized Functional Form (GFF) of Garland and Raccah. We seek to determine if the high current condition causes errors in estimation of the band gaps or broadening parameters. The results of our studies appear in Table 2.

b. How do E_1 values measured at high current compare to low current, using the full GFF (1&2&3)D theory?

(1) Effects of electron beam current density on energy gap estimates.

For the case in which samples have been mounted within a Cu gasket, the results of Table 2 suggest that the 95 K estimate of E_1 is essentially unaffected by the electron beam current parameter. This result is obtained regardless of the clear change from third derivative to first derivative lineshape of the EBER spectra. By comparing the (1&2&3)D fits at 0.6 and at 8 μA, we find that the E_1 values are 2.5596 and 2.5644 eV, respectively, with a difference of 0.0048 eV. The resulting E_1 values lie within the joint standard deviation (we define the joint standard deviation here to mean the square root of the sum of the squared individual standard deviation values) (0.0116) of the E_1 measurements, which is 2.5608 eV. As a result, the higher electron beam current conditions do not measurably affect the E_1 energy value at 95 K when the full GFF (1&2&3)D is used consistently. This result may also be interpreted to mean that the average surface temperature of the sample has not been significantly affected by the electron beam.

Similarly, in comparing the (1&2&3)D fits only for the case of the $E_1+\Delta_1$ peak, the values from the low current (3.1784) and the high current value (3.2143) differ by only 0.0359. This is 2.4 joint standard deviations of 0.0150.

Table 2. Results of fitting MCT data to GFF model. Comparison of third derivative to GFF (1&2&3 D) fits.

Beam Current (μA)	E_1 (eV)	$E_1+\Delta_1$ (eV)	Γ_{E1} (meV)	$\Gamma_{E1+\Delta 1}$ (meV)	Model (derivatives)
			Fits using third derivative only		
a) 0.6	2.5772		134.8		3
	{0.0052}		{5.2}		
b) 0.6	2.5612		116.0		3
	{0.0028}		{2.4}		
c) 0.6	2.5800	3.2027	125.1	177.9	3
	{0.0035}	{0.0063}	{3.4}	{6.3}	
ave:	2.5728	3.2027	125.3	177.9	
std. meas.	0.0083	0.0063	7.7	6.3	
std. joint	0.0038		3.7		
			Fits using first, second, and third derivatives		
a) 0.6	2.5555		109.9		1&2&3
	{0.0054}		{7.3}		
b) 0.6	2.5573		103.2		1&2&3
	{0.0081}		{6.2}		
c) 0.6	2.5661	3.1784	103.8	117.2	1&2&3
	{0.0061}	{0.0137}	{7.1}	{19.6}	
ave:	2.5596	3.1784	105.6	117.2	
std. meas.	0.0046	0.0137	3.0	19.6	
std. joint	0.0065		6.8		
			Comparison of First Derivative and (1&2&3 D) Fits		
d) 8.0	2.5695	3.2032	54.8	71.2	1
	{0.0011}	{0.0016}	{1.1}	{1.7}	
d) 8.0	2.5644	3.2143	89.7	114.3	1&2&3
	{0.0019}	{0.0060}	{5.5}	{10.4}	
ave:	2.5670	3.2088	72.3	92.7	
std meas	0.0025	0.0055	17.5	21.6	
std joint	0.0022	0.0062	5.6	10.5	

Notes:
1. Dimensionalities = 2 for both E_1 and $E_1+\Delta_1$.
2. Temperature = 95 K for all data.
3. Standard error in brackets ({}).

We conclude that no additional uncertainties are incorporated by evaluations of the band gap energies E_1 and $E_1+\Delta_1$ under high electron beam current conditions at 95 K, when the thermal mounting is adequate. The higher signal/noise resulting from the higher electron beam conditions may provide some advantage in reduced error estimates in the cases of higher electron beam currents, and resulting faster data acquisition.

(2) Effects of electron beam current density on broadening parameter estimates.

The estimates of broadening parameter Γ at E_1 are affected more strongly than the energy gap estimates when compared between different electron beam currents, even using the same (full GFF) model. Between the low current (1&2&3)D estimate of Γ (105.6 meV) and the high current value (89.7 meV) is a difference of 15.9 meV. This represents 1.8 joint standard deviations of 8.7 meV.

Further, the estimates of Γ at $E_1+\Delta_1$ appear to be less affected between different electron beam currents, using the same (full GFF) model. Between the low current (1&2&3)D estimate of Γ (117.2 meV) and the high current value (114.3 meV) is a difference of 2.9 meV. This represents much less than even the lowest standard deviation of 10.4 meV.

These results are interesting, because the effects of high electron beam current are opposite from those anticipated. The Γ term represents carrier scattering and it thus increases with sample temperature and defect density. As a result, Γ may be anticipated to enlarge by increasing the electron beam current density. However, the data in Table 2 controverts this hypothesis. We note that the estimated standard deviation from the high current measurement is lower than that of the low current measurements, presumably due to the higher signal/noise obtained.

c. How do E_1 values estimated with third derivative compare to (1&2&3)D at low electron beam current densities?

(1) Effects of fitting model on energy gap estimates.

The results also show that the effect of adding all three derivative components changes the estimation of the E_1 and $E_1+\Delta_1$ energies very slightly. For the E_1 peak, the difference between the values from the third derivative value (2.5728) and the (1&2&3)D value (2.5596) is only 0.0132 eV, which is three times the joint standard deviation of 0.0045. For the case of the $E_1+\Delta_1$ peak, the third derivative value (3.2027) and the combined value (3.1784) differ by only 0.0243. This is 1.6 joint standard deviations of 0.0151. These appear to be significant differences (almost 3 standard deviations) in band gap energy estimates, but these absolute differences in estimated band gap energy are negligible considering the approximate error in *x* value.

(2) Effects of fitting model on broadening parameter estimates.

In contrast, the evaluation of the broadening parameter Γ appears to be very strongly affected by the choice of theoretical fitting model. For the E_1 peak, the difference between the values from the third derivative value (125.3 meV) and the combined (1&2&3)D value (105.6 meV) is 19.7 meV, which is 2.4 joint standard deviations of 8.26 meV. The difference in Γ between the two cases is quite clear, for it represents a fractional difference of 17% of the average value of 115 meV.

For the case of the $E_1+\Delta_1$ peak, the values from the third derivative value (177.9 meV) and the combined (1&2&3)D value (117.2 meV) show a difference of 60.7 meV. This is about 3 joint standard deviations of 20.5 meV. Again, the difference in Γ between the two cases is quite clear; it represents a fractional difference of 41% of the average value of 147 meV.

Therefore, we must hold the values of Γ to be extremely uncertain when compared between different theoretical models. Although the lowest estimated standard deviations are obtained from the limited third derivative model, the differences between subsequent spectral fits (joint standard deviations) are much lower for the full GFF (1&2&3)D fits. Although the differences were statistically significant in the case of the energy gap estimates, they were argued to be of little real consequence in their effect on the estimate of the MCT composition. However, in the case of broadening parameter Γ, the attribution of crystal quality to Γ value is much more significant due to the high fractional differences between fitted values. We conclude from this study that the full GFF (1&2&3)D fit must be used consistently in evaluating the EBER data, even at low electron beam current densities.

d. How do E_1 values estimated with first derivative compare to (1&2&3)D at high electron beam current densities?

(1) Effects of fitting model on energy gap estimates.

At high electron beam current densities, we compare the effects of neglecting the third derivative component of the theory (keeping only the first derivative component), to the full GFF. The results show that the effect of adding all three derivative components changes the estimation of the E_1 and $E_1+\Delta_1$ energies very slightly. For the E_1 peak, the difference between the values from the first derivative value (2.5695) and the (1&2&3)D value (2.5644) is only 0.0051 eV, which is two times the joint standard deviation of 0.0025. For the case of the $E_1+\Delta_1$ peak, the first derivative value (3.2032) and the combined value (3.2143) differ by only 0.0111. This is two joint standard deviations of 0.0055. These appear to be insignificant differences (below three standard deviations) in band gap energy estimates, and these absolute differences in estimated band gap energy are negligible considering the approximate error in x value.

(2) Effects of fitting model on broadening parameter estimates.

In this section, we explain why we have found the full GFF model, incorporating first, second, and third derivative components of the lineshape, to be required for consistent evaluation of the EBER results. We use as a basis the concept that the energy gap E_1 and the broadening parameter Γ are intrinsic properties of the MCT sample at the position and analysis temperature used. Therefore, choices of model and analysis condition must provide estimated values of these intrinsic parameters within the statistical uncertainty of the measured values. Models which give grossly differing values from multiple EBER spectra of the same sample cannot be considered appropriate.

As observed comparing third derivative to GFF fits, the evaluation of the broadening parameter Γ appears to be very strongly affected by the choice of theoretical fitting model for first derivative to GFF models. For the E_1 peak, the difference between the values from the first derivative value (54.8 meV) and the combined (1&2&3)D value (89.7 meV) is 34.9 meV. This corresponds to 6.2 joint standard deviations of 5.6 meV. The difference in Γ between the two cases is quite clear, for it represents a fractional difference of 48% of the average value of 72.3 meV. Most importantly, it is clear that the GFF (1&2&3)D fit most closely matches the low electron beam results discussed above.

For the case of the $E_1+\Delta_1$ peak, the values from the first derivative value (71.2 meV) and the combined (1&2&3)D value (114.3 meV) show a difference of 43.1 meV. This is about 4.1 joint standard deviations of 10.5 meV. Again, the difference in Γ between the two cases is quite clear; it represents a fractional difference of 46% of the average value of 92.7 meV. Once again, the GFF (1&2&3)D fit most closely matches the low electron beam results discussed above.

As we found above in the low electron beam current case, in the case of high electron beam current we must hold the values of Γ to be extremely uncertain when compared between different theoretical models. Although the lowest estimated standard deviations are obtained from the limited first derivative model, the differences between low and high electron beam current spectral fits (joint standard deviations) are much lower for the full GFF (1&2&3)D fits. To reiterate, in the case of broadening parameter Γ, the attribution of crystal quality to Γ value is much more significant due to the high fractional differences between fitted values. We conclude from this study that the full GFF (1&2&3)D fit must be used consistently in evaluating the EBER data, both at low and high electron beam current densities.

4. STUDIES OF EBER DETECTION OF ELECTRON BEAM EFFECTS ON THE MCT SURFACE AND CALCULATION OF THERMAL EFFECTS.

a. Effects of the electron beam on surface composition.

Given the low thermal conductivity of MCT,[11] we anticipated that the electron beam may cause surface heating and lead to a thermoreflectance signal, instead of the electroreflectance (ER) signal desired. The concerns were two-fold.

First, we were uncertain that the correct energy gap E_1 and broadening parameter Γ could be obtained accurately from the TR signal, due to the large energy extent of the peaks. Secondly, we became concerned that the electron beam may induce some surface modification which would affect the higher temperature EBER measurements. We expected that this modification would be Hg loss due to electron beam induced sublimation.

From earlier work performed on MCT, we anticipated that high electron beam current densities may affect the MCT by causing sublimation of Hg in vacuum. The current densities employed in the earlier studies were of order 80 μA into an area of about 0.5 mm^2. The electron beam voltage is typically 240 V. These conditions correspond to a current density of 19.2 mA/cm^2, and a power density D_P of 7.68 W/cm^2.

The effects of electron beam heating of $Hg_{1-x}Cd_xTe$ have been studied by earlier researchers. Shih, *et al.*[12] describes that Hg loss extends only a few monolayers before Te on the surface retards further Hg loss, but that sample heating may extend several thousand Å; surfaces become p-type as Hg is lost. The mechanism of Hg loss was found to be only related to heating, and not to electron stimulated desorption (ESD), which would have required a minimum electron energy.

We had earlier observed a slight but detectable change in the determined E_1 MCT peak energy upon repeated EBER analysis cycles between 90 K and 300 K, as shown in Figures 9 through 11. In this study, we had focussed the electron beam to its smallest functional diameter of 0.5 mm, and used an average electron beam current of 50 μA. This provided the strongest EBER signals, but also caused the most intense heating of the sample by the electron beam. We concluded that EBER analysis under these most severe conditions would cause some detectable surface composition changes in MCT above a temperature of 210 K.[13]

Under conditions of lower electron beam current we find that surface modification is observed only at much higher sample temperatures. Figures 12 to 14 show a series of EBER measurements of a single MCT sample, which are listed in Table 3A. Figure 13 shows that the 90 K transition increases significantly in observation #15, which followed the 400 K measurement. The temperature dependence from these measurements, also listed in Table 3B, is $\partial E_1/\partial T = -3.59\ (\pm 0.25) \times 10^{-4}$ eV/K. Figure 13 shows that both the E_1 and the $E_1+\Delta_1$ transition energies appear to change consistently with temperature. Indeed, as Table 3B also shows, $\partial \Delta_1/\partial T$ is measured for this sample to be only $4.23\ (\pm 2.8) \times 10^{-5}$ eV/K.

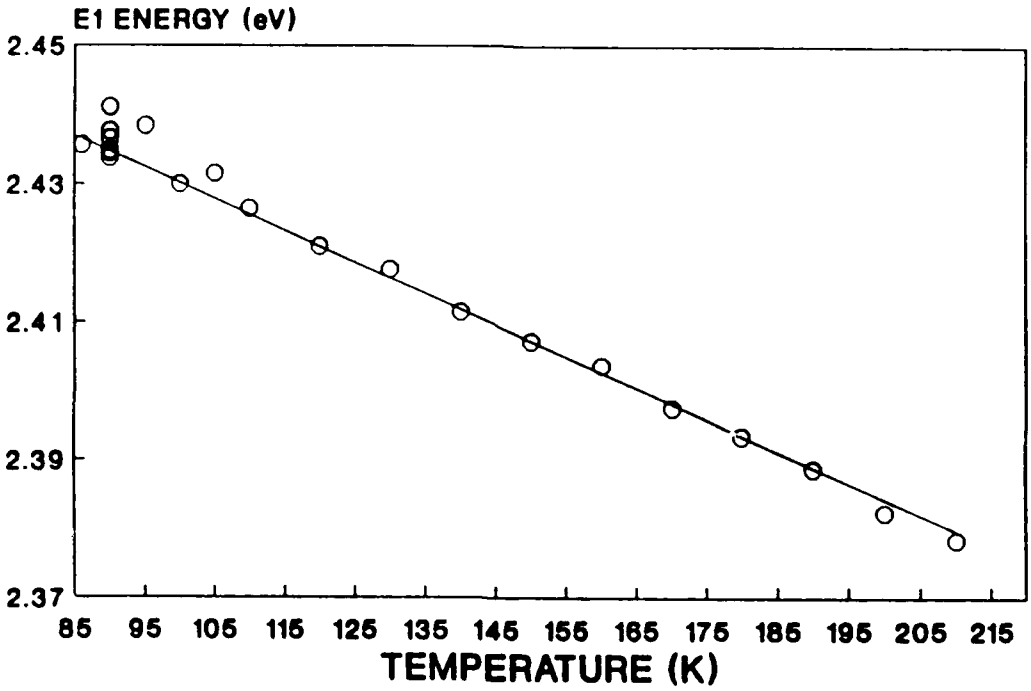

Figure 9. High electron beam current (40 μA) MCT study showing the temperature dependence of the E_1 band gap. The back of the sample was mounted to a copper holder with silver paint. The data is fit to a linear E_1 temperature dependence ($\partial E_1/\partial T$) of -4.582 (±0.062) x 10^{-4} eV/K.

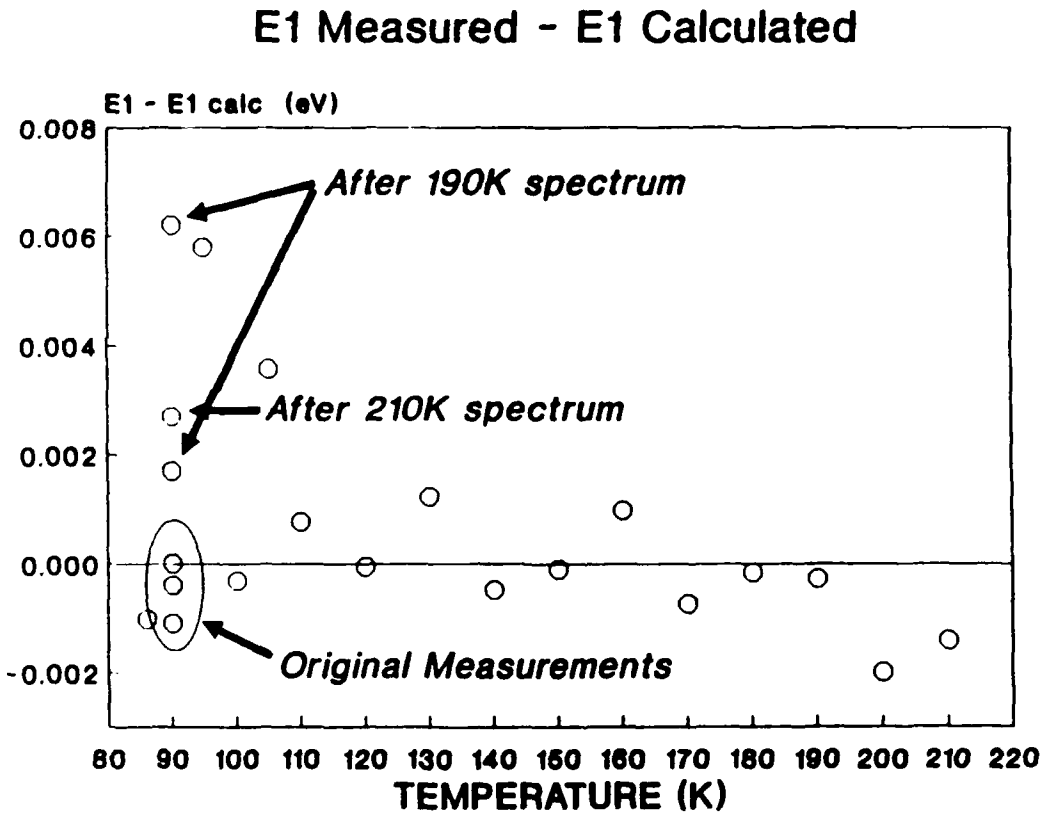

Figure 10. Deviations from linearity in Figure 6.

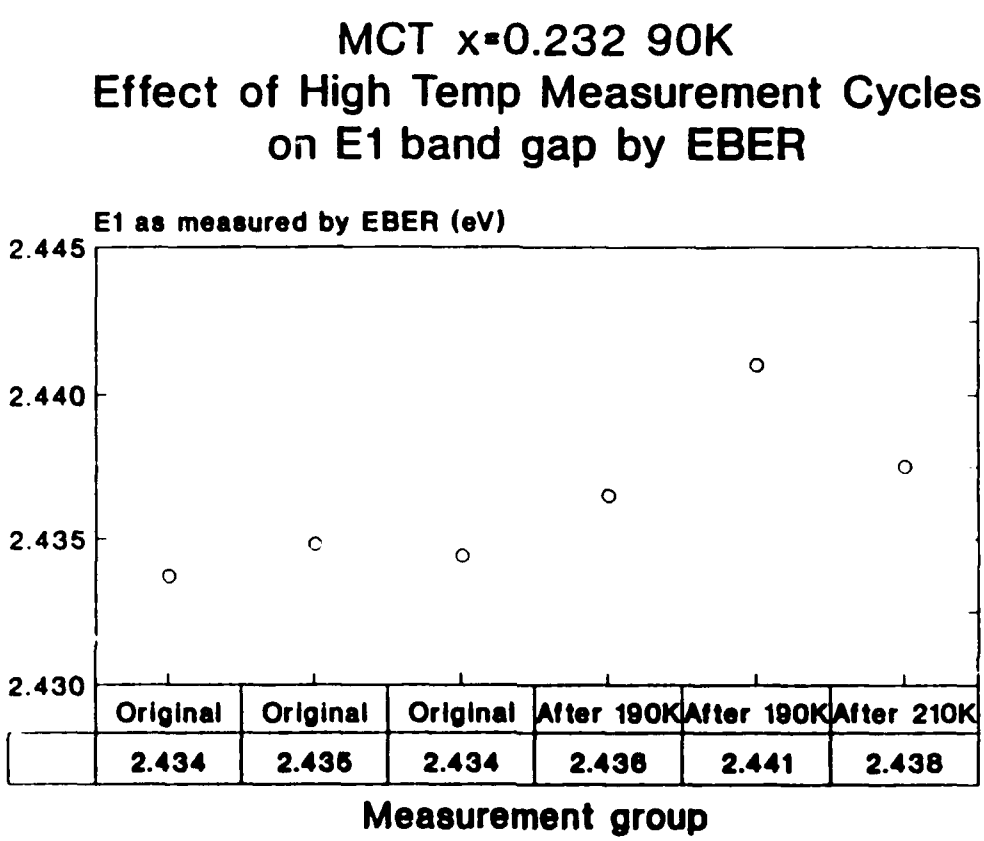

Figure 11. The MCT study showing changes in 90 K E_1 energies after EBER analysis at 190 K and 210 K under high electron beam current (40 μA) conditions. The data suggests that Hg is lost from the surface, resulting in a net increase in Cd and an increase in E_1 band gap energy.

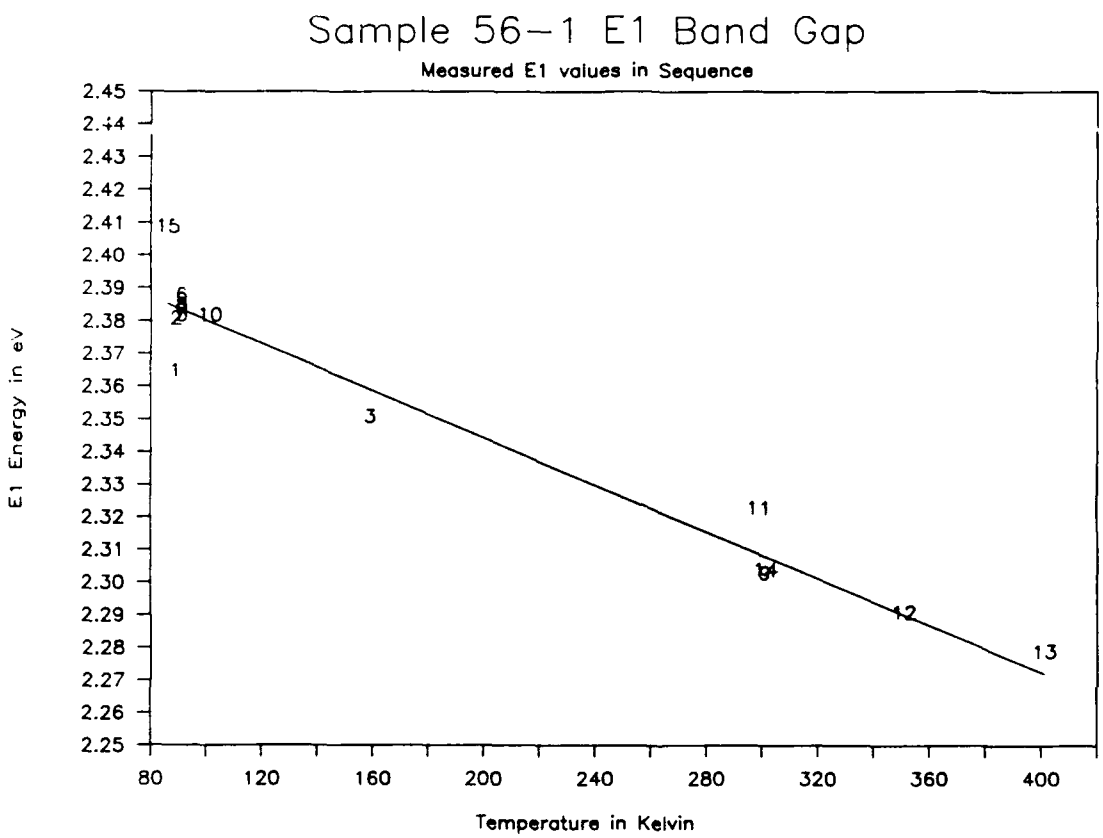

Figure 12. The EBER study of sample 56-1 (MCT epi on CdTe) showing a sequence of E_1 band gap measurements (listed in Table 4). The figure shows that the 90 K transition increases significantly in point #15, which followed the 400 K measurement. The temperature dependence from these measurements, also listed in Table 4, is $\partial E_1/\partial T = -3.59\ (\pm 0.25)\ 10^{-4}$ eV/K.

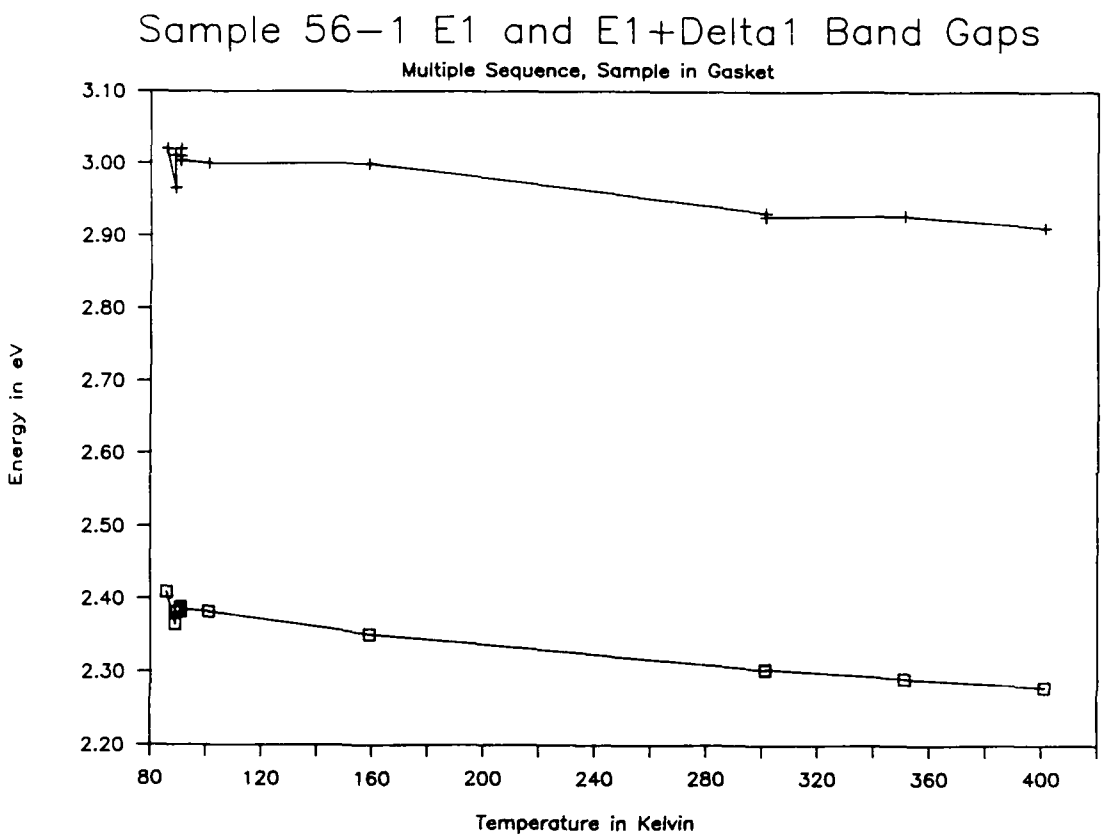

Figure 13. The EBER study of sample 56-1 (MCT epi on CdTe) showing both the E_1 and the $E_1+\Delta_1$ transition energies. $\partial\Delta_1/\partial T$ is measured for this sample at only 4.23 (±2.8) x 10^{-5} eV/K, demonstrating that the two transitions have essentially identical temperature dependence.

Table 3A. Results of sequential study of E_1, $E_1+\Delta_1$ and Δ_1 bandgaps.

File	Temp (K)	E_1 (eV)	$\Gamma[E_1]$ (meV)	$E_1+\Delta_1$ (eV)	$\Gamma[E_1+\Delta_1]$ (meV)	Δ_1 (eV)
1	89	2.365	37.9	2.966	106.0	0.601
2	89	2.381	62.2	3.011	85.8	0.630
3	159	2.351	65.7	3.000	87.1	0.649
5	91	2.382	55.7	3.010	80.0	0.628
6	91	2.388	53.9	3.020	81.7	0.632
7	91	2.383	54.4	3.004	82.2	0.621
8	91	2.385	56.2	3.004	78.6	0.619
9	301	2.303	51.7	2.932	111.0	0.629
10	101	2.382	32.8	3.000	58.6	0.618
11	299	2.323	74.3	3.005	127.0	0.682(?)
12	351	2.291	53.7	2.928	106.0	0.637
13	401	2.279	60.2	2.912	141.0	0.633
14	301	2.304	47.7	2.927	91.0	0.623
15	86	2.409	41.1	3.020	100.4	0.611
					ave:	0.6254
					std. dev.	0.0116

Note:
1. All data taken on sample 56 with copper gasket.

Table 3B. Linear regression analysis: E(T) = A + BT (excluding File 11).

	E_1	$E_1+\Delta_1$	Δ_1
A (eV)	2.4160	3.0342	0.6182
Standard Error of A	0.0101	0.0152	0.0115
B (eV/K)	-3.59E-04	-3.17E-04	4.23E-05
Standard Error of B	2.45E-05	3.68E-05	2.78E-05
R Squared	0.9513	0.8709	0.1732
No. of Observations	13	13	13
Degrees of Freedom	11	11	11

These measurements shown in Figure 14 demonstrate that a significant change in E_1 energy followed the measurements at 300, 350, and 400 K, but not earlier 300 K measurements. This result is understandable from both the lower thermal conductivity of MCT as temperature is raised, and the fact that less additional electron beam energy is needed for sublimation of the Hg when the incipient thermal energy is high.

b. Calculation of the electron beam effects on surface temperature.

Several pertinent calculations of the effects of electron beams on solids have been published. We apply the salient results of several articles as follows. If the electron beam diameter is much smaller than the distance between the irradiation point and the isothermal mounting, as in an SEM, for example, the surface temperature rise from a moving electron beam has been described as[14,15]:

$$\Delta T = T_m - T_s = P/[(8\pi)^{1/2} K_s r_b] \qquad (1)$$

where K_s is the thermal conductivity, r_b the beam diameter, T_m the temperature at the center of the beam, and T_s the substrate temperature. The P is the power of the electron beam--that is, the product of the current and voltage. Using the published[11,16] thermal conductivity K_s of between 8 and 35 mW/cm-K, and a beam diameter of 1 mm, we estimate the increase in surface temperature to be between 0.014 K/μA and 0.0613 K/μA. Employing average current values of 1 μA to 100 μA results in an estimated temperature increase of between 0.1 K and 6.0 K. The maximum surface temperature would be double the average value.

In the case of a semi-infinite solid, the effect of an electron beam on the surface temperature has been treated by Pittaway.[17] In the Pittaway analysis, the temperature at the surface, and at the center of a Gaussian electron beam is

$$\Delta T = \{D_p/K_s d\pi^{3/2}\} \tan^{-1}(2\lambda^{1/2}) \qquad (2)$$

where

$$\lambda = \kappa t'/d^2 \qquad (3)$$

where d is the Gaussian decay parameter for the electron intensity (typically 0.5 mm), κ is the thermal diffusivity, and t' is the time that the electron beam is irradiating the sample. Of course, if the surface cools to the substrate temperature during each cycle, then t' is the inverse frequency of the electron beam. From published literature,[18] we estimate that the thermal diffusivity κ of MCT at 300 K has the value 0.007 to 0.03 cm^2/sec, becoming smaller as the Cd content or the temperature increases. As this analysis contains the irradiation time within the arctangent function, it allows us to calculate the frequency dependence of the heating, confirming the experimental results. Table 4 shows the effects of frequency and peak electron beam current at two typical electron beam diameters. These calculations compare favorably to the experimental results in Table 1.

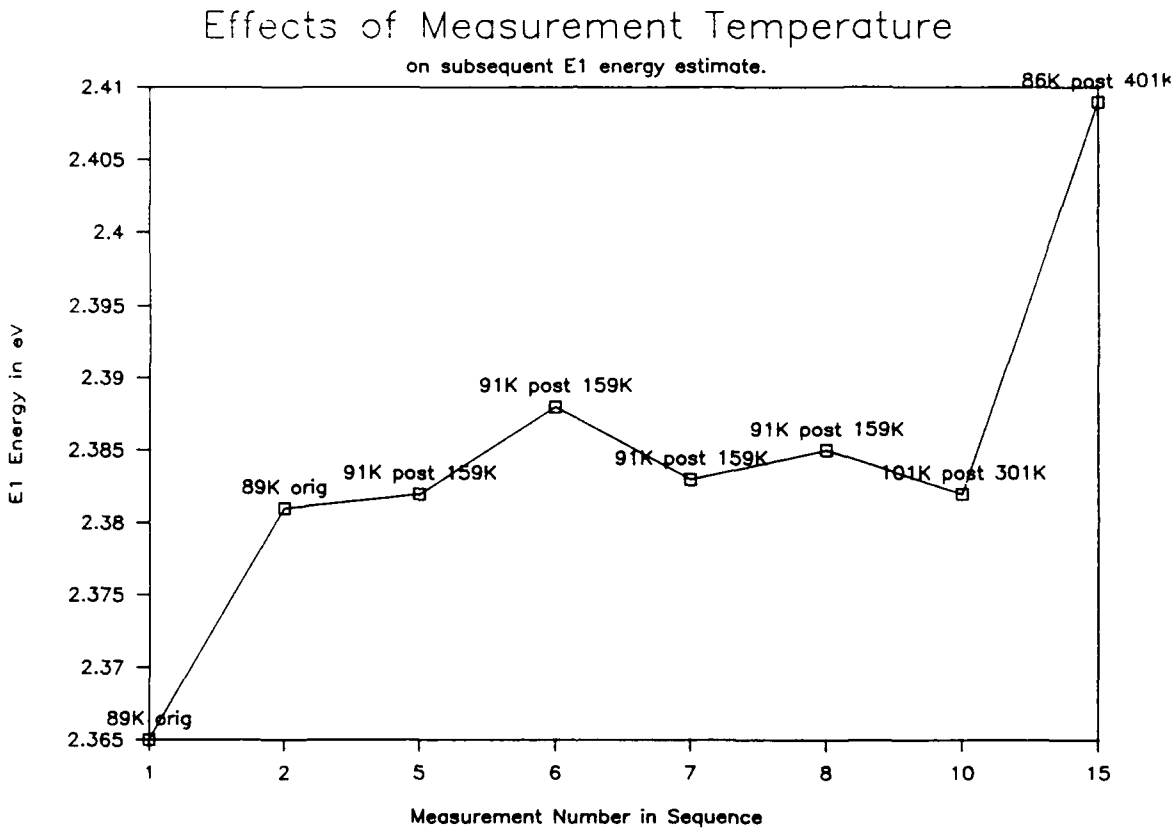

Figure 14. Results of EBER analysis of a sample of MCT under low electron beam current density conditions. We observe that the E_1 energy measured at 95 K changed by a negligible degree after cycling even to 300 K under electron beam irradiation, in ultra-high vacuum. However, following measurements at 350 and 400 K, there was an increase in the E_1 transition energy corresponding to Hg loss from the surface.

Table 4. Peak surface temperature rise from electron beam heating.

Diameter (mm)	Peak Current (μA)	ΔT @ 600 Hz (K)	ΔT @ 200 Hz (K)
0.5	200	5.9-13.1	8.9-21.8
	100	3.0- 6.6	4.5-10.9
	10	0.3- 0.7	0.4- 1.1
	1	0- 0.1	0- 0.1
1.0	200	1.6-3.3	2.6-5.7
	100	0.8-1.7	1.3-2.9
	10	0.1-0.2	0.1-0.3
	1	0	0

If the diameter of the electron beam is of the same order as the sample thickness, then by analogy to electrical resistance problems, we can also estimate the increase in surface temperature to be:

$$\Delta T = D_p L/K_s \tag{4}$$

where D_p is the power density of the electron beam (7.68 W/cm^2 at 80 μA and 240 V) and L is a mean thermal distance between the electron beam irradiation and the isothermal sample mount. Using a value of L of 1 mm provides an estimated temperature increase of between 22 and 96 K. For comparison, the surface of GaAs would rise by only 1.7 K under the same conditions. Dropping the electron beam current to 1 μA would change the surface temperature by only 0.3 K to 1.2 K. It is this large effect which we believe introduces the measured thermal modulation, and simultaneously introduces error in the estimation of the sample surface temperature.

c. Observations of differences in lineshape between E_1 and $E_1+\Delta_1$.

As a final comment about the TR mechanism, we discuss differences in lineshape observed between the E_1 and the $E_1+\Delta_1$ peaks. In ER, the measurement depth is limited by the smaller of the electric field or the light penetration depths. In the case of MCT samples studied, the measurement depth is limited by the light penetration--about 500 Å for the E_1 peak, and 300 Å for the $E_1+\Delta_1$ peak. For this reason, the $E_1+\Delta_1$ peak shows strong first derivative (TR) component, even though the E_1 peak shows primarily a third derivative (ER) component in our EBER spectra taken at low electron beam currents. Again, these qualitative features support the TR mechanism over alternative modulation mechanisms for the generation of first derivative lineshapes in EBER analyses of MCT.

d. Determination of optimal EBER operating conditions for MCT analysis.

We have determined low electron beam current density operating conditions for the EBER instrument so that sample modification (Hg sublimation) from the surface of the sample is unmeasurably small. The lower current densities are achieved by enlarging the electron beam and light beam on the surface, to spread out the energy of both beams. We have found that an electron beam spot of 3 mm diameter or larger provides adequate relief from Hg loss.

The results of our study appear in Figure 14. These results show that repeated measurements at 90 K give the same energy measurement as those taken before repeated cycles of the sample to 300 K, under the lower electron beam current density conditions. This test assured us that subsequent measurements of MCT samples would not measurably affect our results.

5. INVESTIGATIONS OF THE TEMPERATURE DEPENDENCE OF THE E_1 BAND GAP OF MCT BY EBER.

After determining optimal EBER operating conditions for MCT, we have investigated eight samples of MCT, ranging from pure HgTe ($x = 0$) to CdTe ($x = 1$). We have obtained spectra from all samples over the E_1 region, at nominal temperatures between 100 K and 400 K.

a. Results of temperature dependence.

Upon analysis of our data, we found unexpectedly low values for the temperature dependence $\partial E_1/\partial T$. The most recent study by Berlouis *et al.*[19] gives a value of -6.6 (±0.5) x 10^{-4} eV/K for MCT with x between 0.23-0.36. The Berlouis study of three samples also showed that a sample grown epitaxially on CdTe had a larger temperature dependence of the E_1 band gap than the other two bulk samples. Our values for samples in the clip mounting, appearing in Table 5, ranged from -0.905 to -5.600 x 10^{-4} eV/K. Using silver-paint mounting for good thermal conductivity, (but large electron beam currents,) we had obtained a value of -4.58 (±0.06) x 10^{-4} eV/K from studies of $x = 0.23$ MCT. Our values for samples in the clip mounting lie significantly lower than these literature values, and caused us to consider instrumental conditions as a cause.

b. Discussion of results: effects of sample surface temperature.

We have estimated the effects of sample stage temperature error on the calculated $\partial E_1/\partial T$ values. Temperatures are currently measured to 1 K precision and 2 K accuracy by an iron-constant thermocouple (TC). Additionally, we have installed an RTD (resistance thermometer device) for

Table 5. Temperature dependence of E_1 band gap on MCT mount.

Mount	Sample	x-value (Raccah formula)	$\partial E_1/\partial T$ (10^{-4} eV/K)
Clip	HgTe	0.000	-5.41
Clip	56	0.238	-3.36
Clip	53	0.247	-0.91
Clip	50	0.274	-3.49
Clip	52	0.342	-3.90
Clip	CdTe	1.000	-5.97
Ag Paint	N.A.	0.232	-4.58
Cu Gasket[a]	52	0.333	-7.78
Cu Gasket[b]	52	0.313	-8.49
Cu Gasket[c]	52	0.312	-6.691
Cu Gasket[d]	52	0.260 (±0.038)	-9.19 (±2.12)

[a]Low current 0.6 μA.
[b]Medium current 6.0 μA.
[c]Rerun at low current 0.6 μA.
[d]E_1(298 K) = 2.3341 (±0.0368) eV, E_1(97 K) = 2.5198 (±0.0218) eV, rerun at low current 0.6-2.0 μA .

correlated readings of the sample stage mperature. When temperatures between 100 K and 300 K are used for estimation of $\partial E_1/\partial T$, the deviation induced in paired measurements affects the $\partial E_1/\partial T$ results by only 5×10^{-6} eV/K which is 1% of the estimated value. Therefore, we feel that temperature measurements with greater than 2 K accuracy are not needed for this experiment.

Still, we suspected that our sample holder, with a single clip mount for the MCT, shown in Figure 15, was insufficient to guarantee cold upper surfaces. We believed that the radiation from the electron beam and from the room temperature walls of the vacuum system was sufficient to heat the upper 300 Å of the MCT surface, so that the temperature of the measured surface was not that of the copper sample holder. We then constructed a new sample holder shown in Figure 16 with a surface copper gasket. The gasket provides both an upper surface thermal contact, and better thermal contact to the copper sample holder. We note that even this case is still insufficient to guarantee the temperature of the sample surface, due to radiation heating from the probe light beam and the electron beam. This issue is inherent to electroreflectance measurements at the high energy band gaps of any crystalline material, where the light penetration is so shallow.

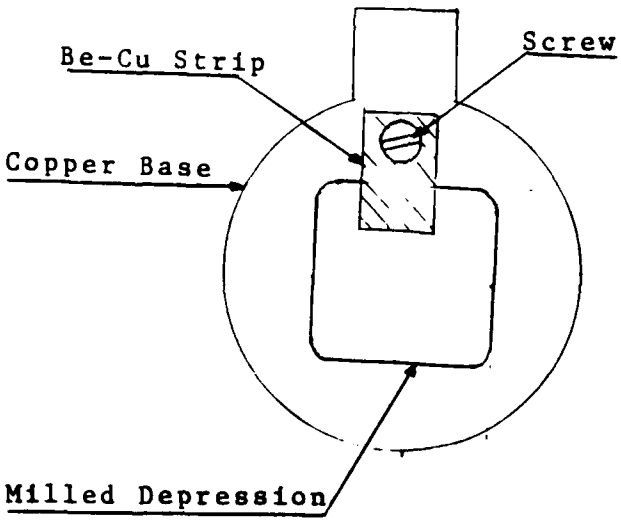

Figure 15. Original sample holder with single Cu-Be clip.

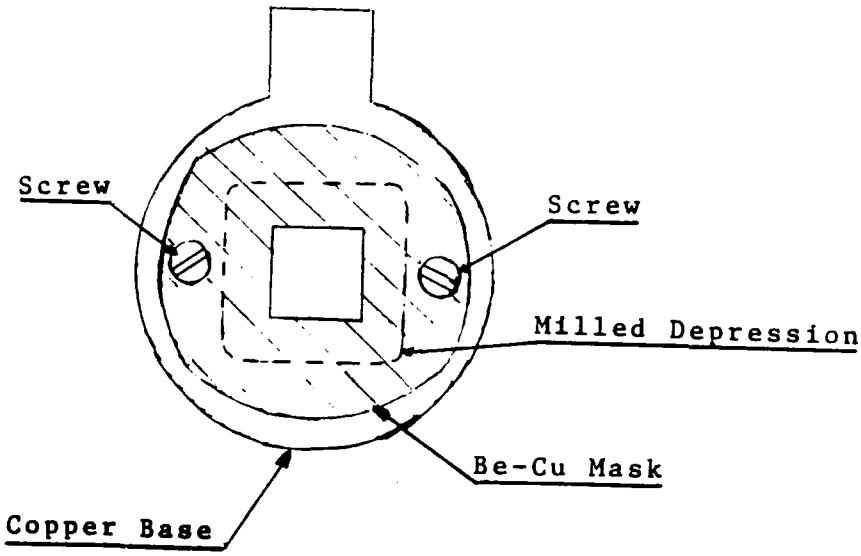

Figure 16. Revised sample holder with Cu-Be surface gasket.

c. **Results of experiments with new sample holder.**

(1) Results at the E_1 band gap.

With the new sample holder, we re-ran the epitaxial MCT on CdTe sample 52, and found a value commensurate with that of Berlouis. We found that at low electron beam currents of 0.6 μA, at 96 K, E_1 = 2.5662 eV, and at 300 K, E_1 = 2.4057 eV. This results in an estimate of $\partial E_1/\partial T$ of -7.79 x 10^{-4} eV/K, using the Raccah formula, x = 0.333, for this sample measurement. Repeated measurements on the same sample, but at a later time and a different position, provided a value of -9.19 (±2.12) x 10^{-4} eV/K, and an x value estimate of 0.26 (±0.04). Therefore, our value goes beyond the upper limit of $\partial E_1/\partial T$ found by Berlouis *et al.* (-6.6 (±0.5) x 10^{-4} eV/K). A subsequent measurement of the same sample, at electron beam currents of 10 μA, gave an estimated $\partial E_1/\partial T$ of -6.69 x 10^{-4} eV/K, which lies within the range specified by Berlouis *et al.*

Although we can conceive of many reasons why our estimates of the $\partial E_1/\partial T$ value may be erroneously low (by Hg loss going to high temperature, or by insufficient heating of the sample), we foresee only two reasons why the temperature dependence may be estimated too large. First, increased surface radiation heating at higher temperatures would cause an artificially high value to be obtained. This may occur due to the reduced thermal conductivity of MCT as the temperature is raised. We must secondly consider that the epitaxial MCT on CdTe is a strained system, and that the E_1 and $E_1+\Delta_1$ band gap energies will be responsive to strain in the epitaxial material. Therefore, the temperature dependence of the epitaxial MCT may be larger than that of bulk material. Of the three samples studied by Berlouis *et al.*, the one epitaxial sample did demonstrate the largest temperature dependence of the E_1 transition.

(2) Results at the $E_1+\Delta_1$ band gap.

We have found no literature values for either the value of the $E_1+\Delta_1$ band gap which lies near the E_1 transition energy, nor for its temperature dependence. Our data on the $E_1+\Delta_1$ band gap appears in Tables 2, 3, and 6. From Table 2, the estimated Δ_1 value ranges from 0.6188 to 0.6418 at electron beam currents of 0.6 μA and 8.0 μA respectively, for sample 52 at 95 K. From Table 3, we found that for sample 56, the value of Δ_1 was 0.6254 (±0.0116) eV and the Δ_1 splitting has a small positive temperature dependence--about 5 x 10^{-5} eV/K. In contrast, as shown in Table 6 for sample 52, we have found the splitting to be somewhat larger but still positive--about 2 x 10^{-4} eV/K. In both cases, the $E_1+\Delta_1$ band gap has a temperature dependence of about -5 x 10^{-4} eV/K.

Table 6. Temperature dependence of MCT $E_1+\Delta_1$ and Δ_1 band gaps. (All from epitaxial sample 52 with Cu gasket mount)

Band gap	Sample	x-value (Raccah formula)	$\partial(E_1+\Delta_1)/\partial T$ (10^{-4} eV/K)	$\partial\Delta_1/\partial T$ (10^{-4} eV/K)
$E_1+\Delta_1$	current 0.6 μA	0.333	-4.078	+3.174
$E_1+\Delta_1$	current 6.0 μA	0.313	-6.074	+2.721
$E_1+\Delta_1$	rerun 10.0 μA	0.312	-4.209	+2.482

6. INVESTIGATIONS OF THE SURFACE TREATMENTS OF BULK CdTe AT THE E_0 BAND GAP BY EBER.

In work closely related to the analysis of MCT, we have conducted studies of CdTe bulk samples. Our studies were intended to show differences in the quality of CdTe samples which had been prepared with different surface treatments. We chose to study the E_0 band gap transition, because the penetration depth is quite large, and the potential for excitonic effects is strongest. The exciton is very sensitive to defects and impurities due to its large volume--sharp excitonic transitions correspond to long exciton lifetimes and therefore high quality.

As Figure 17 shows, three samples of [111]-oriented CdTe were studied. The three possessed (1) a mechanical 0.3 μm diamond polish, (2) an alternative "diamond turned" surface and (3), a combination of mechanical and chemical polish. Figures 17a, b, and c show EBER spectra of the three samples, at 300 K. Sample 1 has the broadest optical transitions, followed by sample 2 and then by sample 3 which has the sharpest transitions. The transitions have been initially modeled as excitonic, but may also be fitted to interband transitions. Using consistent models for all three cases shows that the broadening parameters Γ for the sharpest transitions in the three cases follow the expected trend: 31.4 meV for (1), 31.0 meV for (2), and 10.8 meV for (3). The peak energies also appear to increase from 1.464 eV to 1.494 eV to 1.511 eV. This indicates that the effects of purely mechanical polishing may be to introduce defect states below the band edge.

7. STUDIES OF GaAs AND RELATED COMPOUNDS.

As we have recognized the difficulties of studying MCT with EBER, we have expanded our studies to encompass GaAs and related materials where the associated analysis issues (shallow light penetration, low thermal conductivity) are less severe. Several of these studies which we describe briefly below have been presented at scientific meetings or submitted for publication.

Firstly, we have successfully used EBER to examine single GaAs/AlGaAs quantum wells. Numerous results of this study are detailed in the attached paper, which has been presented to the Electronic Materials Conference and submitted

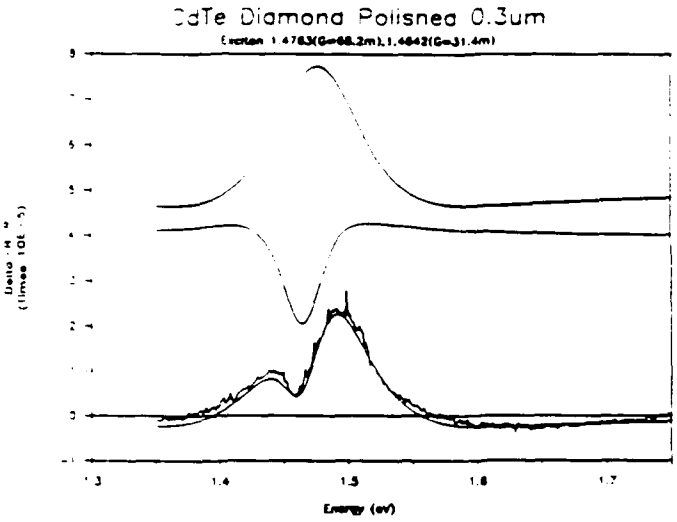

a.

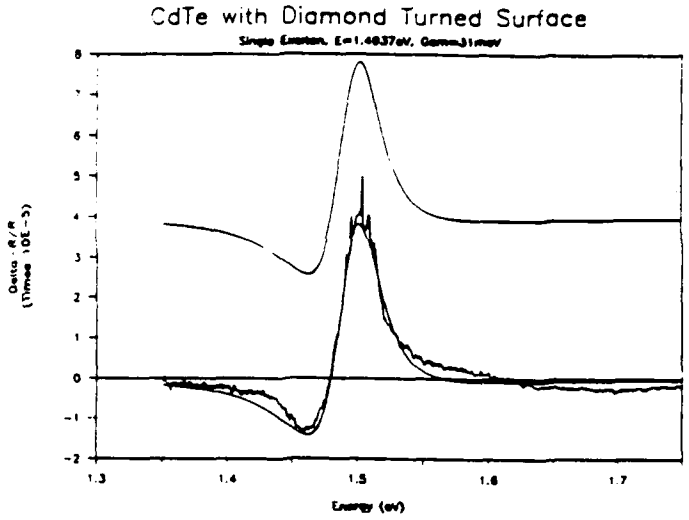

b.

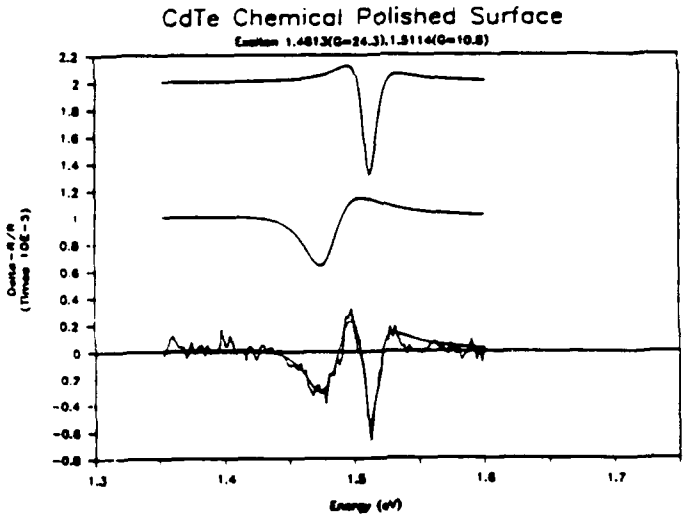

c.

Figure 17. EBER spectra of three samples of [111]-oriented CdTe at 300 K. The three CdTe surfaces had (a) a mechanical 0.3 μm diamond polish, (b) an alternative "diamond turned" surface and (c), a combination of mechanical and chemical polish.

to the Journal of Electronic Materials. We have found evidence for many intersubband transitions between both bound and unbound levels of single quantum wells, and using the rectangular barrier model, we have estimated the conduction band offset parameter Q_c to be nearly 0.62 for the GaAs/AlGaAs system.

Secondly, we have investigated many qualities of GaAs bulk material, and presented data at the American Physical Society Meeting in St. Louis. Working with collaborators at AT&T Bell Laboratories and Aerospace Corporation, we have found clear evidence for an optical transition lying nearly 38 meV below the E_0 transition in several samples of semi-insulating GaAs.[20] The origin of this peak has been the subject of recent research by several other groups.

Third, we have developed several new commercial applications of EBER analysis to heterostructures. These structures include HEMTs fabricated of AlGaAs on GaAs and also pseudomorphic HEMTs which contain strained layers of InGaAs. Our EBER spectra of standard HEMT structures have been presented at the November Materials Research Society Meeting in Boston,[21] and our results on pseudomorphic HEMTs in conjunction with researchers at the University of Texas at Austin will be presented at the forthcoming Electronic Materials Conference in Boston.[22]

III. CONCLUSION

This final report summarizes our experimental researches of applications and mechanisms of electron beam electroreflectance (EBER) to $Hg_{1-x}Cd_xTe$ (MCT) and other semiconductor systems. We have investigated the temperature dependence of the E_1 and $E_1+\Delta_1$ optical band gaps of $Hg_{1-x}Cd_xTe$ (MCT) which have earlier been correlated to composition. In general, we find agreement to the temperature dependence results of other researchers. In particular, for an epitaxial test sample of $Hg_{1-x}Cd_xTe$ with $x = 0.32$ we have repeatedly obtained a value of $\partial E_1/\partial T$ of -(6.7 to 8.2) x 10^{-4} eV/K. Our value is slightly larger than, but consistent with, that determined by Berlouis *et al.* (-6.6 (±0.5) x 10^{-4} eV/K). As did Berlouis *et al.*, we find a larger temperature coefficient for epitaxial MCT on CdTe than for bulk MCT, presumably due to the temperature dependence of elastic strain.

Our investigations have also extended to the $E_1+\Delta_1$ band gap which lies nearly 0.63 eV above the E_1 transition energy. Our data suggests that the value of Δ_1 is 0.625 (±0.012), and may have a small positive temperature dependence between about 5 x 10^{-5} eV/K and 2 x 10^{-4} eV/K. The $E_1+\Delta_1$ band gap has a consistent temperature dependence of about -5 x 10^{-4} eV/K.

We have found MCT to be much more sensitive to the intensity of the electron beam current than other crystalline materials such as GaAs or Si, due to the relatively low thermal conductivity of MCT. The strongly "first derivative" lineshape observed at electron beam current densities of 10^{-3} A/cm^2 appears to us most likely a thermoreflectance (TR) component to the modulated reflectance signal, based upon studies of the frequency, electron beam current dependence, and comparison of the E_1 and $E_1+\Delta_1$ lineshapes. The TR component can be minimized at low temperature with much smaller electron beam currents, resulting in a detectable "third derivative" electroreflectance (ER) signal. However, at room temperature we have not successfully obtained ER signals

without a large TR component. We suspect that surface heating by the electron beam raises the sample temperature in the region probed by the light. Primarily for this reason, repeated determinations by EBER of the temperature dependence of the E_1 and $E_1+\Delta_1$ band gap energies demonstrate a rather large variance.

We have studied the effects of electron beam current density and theoretical fit parameters on the estimates of the E_1 and $E_1+\Delta_1$ band gaps and broadening parameters. We find that the complete GFF (first, second, and third derivative) lineshapes provide the most consistent estimates of parameters in either the low or high current regimes. We find that high electron beam current does not significantly affect the estimates of either band gaps or broadening parameters. In fact, at low measurement temperatures, higher beam currents seem to improve the parameter estimates by increasing the signal/noise ratio of the data. Both low and high current density cases demonstrate comparable band gap energy estimates and Γ values for the E_1 and $E_1+\Delta_1$ band gaps of MCT when the full GFF theoretical model is used. The estimates are more varied when the same spectra are fitted with either purely first derivative or third derivative lineshapes alone.

We have also determined experimental conditions for the EBER analysis of MCT which appear to be non-destructive when samples are measured to at least 300 K. We have found that sufficiently low electron beam current densities provide adequate signal for estimation of the E_1 and $E_1+\Delta_1$ peak energies, but relieve concerns about electron beam modification of the sample surface by sublimation of Hg under vacuum. Using the new conditions, we find that changes in E_1 energy are not significant after repeated cycles of an MCT sample to 300 K while simultaneously under electron beam irradiation.

Further, we have collaborated with other researchers on EBER evaluation of MCT growth and dry-etch processes. We have worked with Stanford University students on evaluation of VPE grown MCT on CdTe substrates, revealing optical information about the quality of various MCT epi layers. Compositional variations from dry etching in small (500 μm) square areas of MCT were evaluated for the Army Night Vision Laboratories and Plasmaquest Corporation. We evaluated the lineshapes both inside and surrounding the etch pit, and found no significant differences between the optically measured compositions. This study resulted in a joint publication.[24]

Additionally, we have extended EBER studies to other technologically important crystal systems related to MCT, such as CdTe. In the case of CdTe, which may be used for substrates in MCT epitaxy, we have found correlations between the EBER measurements and sample preparation methods. Our EBER results on other crystalline systems have also been quite encouraging. In the case of GaAs and related compounds, our results have shown promise in the analysis of epitaxial films and heterostructures. These ancillary results are briefly described.

PUBLICATIONS AND PRESENTATIONS

J. E. Spencer, J. H. Dinan, P. R. Boyd, H. Wilson, and S. E. Buttrill, "Stoichiometric dry etching of mercury cadmium telluride using a secondary afterglow reactor," presented at the American Vacuum Society 35th National Symposium and Topical Conference, April 1988. Published in J. Vac. Sci. Technol. **A7**(3) 676-681, 1989.

R. C. Bowman, Jr., P. M. Adams, M. H. Herman, and S. E. Buttrill, "Effects of rapid thermal anneals on boron-implanted GaAs," presented at the Fall 1988 Materials Research Society Meeting, Boston, MA.

R. C. Bowman, Jr., P. M. Adams, J. F. Knudsen, P. A. Dafesh, D. D. Smith, S. C. Moss, M. H. Herman, & I. D. Ward, "Studies of helium ion implantation on the optical and crystal properties of GaAs," presented at Symposium C, Ion Beam Processing of Advanced Electronic Materials, 1989 Materials Research Society Meeting, San Diego, CA.

S. C. Moss, D. D. Smith, J. F. Knudsen, R. C. Bowman, Jr. and M. H. Herman, "Ion implantation and fabrication effects on the linearity of the photocurrent-voltage characteristics of SOS picosecond photoconductive switches," Proceedings of the IEEE Lasers and Electro-Optics Society Annual Meeting, Santa Clara, CA, Nov. 2-4, 1988.

D. D. Smith, J. F. Knudsen, R. C. Bowman, Jr., M. H. Herman and S. C. Moss, "Role of ion implantation induced damage and surface states in the response of gallium arsenide picosecond photoconductive switches," Proceedings of the IEEE Lasers and Electro-Optics Society Annual Meeting, Santa Clara, CA, Nov. 2-4, 1988.

M. H. Herman, I. D. Ward, R. C. Bowman, D. D. Smith, S. C. Moss, and N. Chand, "Observation of impurities in GaAs by electron beam electroreflectance (EBER)," American Physical Society Meeting, St. Louis, MO, March 1989.

M. H. Herman, I. D. Ward, S. E. Buttrill, Jr., and G. L. Francke, "Characterization of III-V semiconductor structures using electron beam electroreflectance (EBER) spectroscopy." presented at the Materials Research Conference in Boston, MA, November 1988. To be published in the Conference Proceedings.

M. H. Herman, S. E. Buttrill, Jr., G. L. Francke, and F. A. Chambers, "Electron beam electroreflectance (EBER) analysis of single $Al_xGa_{1-x}As/GaAs$ quantum wells" presented at the Electronic Materials Conference, Boulder, CO, June 22-24, 1988. Submitted for publication to the Journal of Electronic Materials.

M. H. Herman, S. E. Buttrill, Jr. and G. L. Francke, "Characterization of III-V and II-VI thin films and interfaces using electron beam electroreflectance (EBER) spectrometry." presented at the Electronic Materials Conference, Boulder, CO, June 22-24, 1988.

REFERENCES

1. P. M. Raccah and U. Lee, "Comparative studies of mercury cadmium telluride single crystal and epitaxial," J. Vac. Sci & Technol. **A1**(3), 1587-1592, 1983. Their results in the expression: $E_1(x) = 2.135 + 0.600x + (0.640\ (\pm 0.05))x^2$. For their study, they used HgTe and CdTe and x = 0.5 MCT.

2. M. Cardona, "Modulation Spectroscopy", in Solid State Physics, F. Seitz, D. Turnbull, H. Ehrenreich, eds., Academic Press: New York 1969.

3. D. E. Aspnes, "Third-derivative modulation spectroscopy with low-field electroreflectance," Surface Science **37**, 418-442, 1973.

4. The issue was discussed by P. M. Raccah, J. W. Garland, S. E. Buttrill, Jr., L. Francke and J. Jackson, "Electron beam electroreflectance studies of GaAs and CdTe surfaces," Appl. Phys. Lett. **52**(19), 1584-1586, 1988. See also the Quarterly Report from this research project for a detailed description.

5. For a calculation of heating effects, see P. M. Raccah, J. W. Garland, S. E. Buttrill, Jr., L. Francke and J. Jackson, "Electron beam electroreflectance studies of GaAs and CdTe surfaces," Appl. Phys. Lett. **52**(19) 1584-1586, 1988. Also see I. Broser, R.-A. Hoffman & H.-J. Schulz, "Mechanisms of cathodoreflectance in germanium," Solid State Comm. **8**, 587-591, 1970; and J. H. McCoy & D. B. Wittry, "Electron beam modulated reflectance of germanium," Appl. Phys. Lett. **13**(8), 272-274, 1968.

6. Band-filling has been suggested numerous times in the past. See for example S. F. Pond and P. Handler, "Flatband electroreflectance of gallium arsenide. I. Experimental results," Phys. Rev. **B6**(6), 2248-57, 1972. With regards to MCT, see P. M. Raccah, J. W. Garland, S. E. Buttrill, Jr., L. Franke & J. Jackson, "Electron beam electroreflectance studies of GaAs and CdTe surfaces," Appl. Phys. Lett. **52**(19), 1584-1586, 1988.

7. D. S. Kyser and V. Rehn, "Piezoelectric effects in electroreflectance," Solid State Comm. **8**, 1437-1441, 1967.

8. P. M. Raccah, private communication.

9. I. Broser, R.A. Hoffman and H.J. Schulz, "Mechanisms of cathodoreflectance in germanium," Solid State Comm. 8, 587-591, 1970.

10. J. W. Garland and P. M. Raccah, "Generalized theory of electroreflectance with applications to materials characterization," SPIE 659, 32-43, Materials Technologies for IR Detectors (1986).

11. M. I. Aliev, S. A. Aliev, D. G. Arasly, R. N. Ragimov and T. G. Gadjiev, "Thermal conductivity of $Hg_{1-x}Cd_xTe$ solid solutions," Dokl. Akad. Nauk. Az. SSSR. 34(9), 28-30, 1978. The thermal conductivity of MCT is 0.008 to 0.035 W/cm-K, 16 to 55 times smaller than GaAs (0.44 to 0.55 W/cm-K). Thermal diffusivity is 0.007 to 0.03 $cm^2/(sec\ K)$ at 300 K for $0<x<0.20$.

12. C. K. Shih, D. J. Friedman, K. A. Bertness, I. Lindau, W. E. Spicer and J. A. Wilson, "Electron beam induced Hg desorption and the electronic structure of the Hg depleted surface of $Hg_{1-x}Cd_xTe$," J. Vac. Sci & Technol. **A4**(4), 1997-2001, 1986.

13. C. K. Shih, *et al.*, *ibid.*

14. C. K. Shih, *et al.*, *ibid.*

15. L. G. Pittaway, "The temperature distributions in thin foil and semi-infinite targets bombarded by an electron beam," Brit. J. Appl. Phys. **15**, 967-982, 1967.

16. By comparison, CdTe has a similar thermal conductivity of 55 mW/cm^{-K}. See the compilation by J. L. Schmit, J. Vac. Sci & Technol. **A4**(4), 2141-2149, 1986.

17. L. G. Pittaway, "The temperature distributions in thin foil and semi-infinite targets bombarded by an electron beam," Brit. J. Appl. Phys. **15**, 967-982, 1967.

18. M. I. Aliev, S. A. Aliev, D. G. Arasly, R. N. Ragimov and T. G. Gadjiev, "Thermal conductivity of $Hg_{1-x}Cd_xTe$ solid solutions," Dokl. Akad. Nauk. Az. SSSR. **34(9)**, 28-30, 1978.

19. In particular, see the article by L. E. A. Berlouis, L. M. Peter, M. G. Astles and R. G. Humphreys, "Electrolyte electroreflectance of HgCdTe at low temperatures," Appl. Phys. Lett. **51**(7), 502-504, 1987. They give the value of $\partial E_1/\partial T$ for MCT as -6.6 (±0.5) x 10^{-4} eV/K for x between 0.23-0.36, using EER, from temperatures 156-300 K. They also indicate that earlier values used were about -0.4 meV/K x 10^{-4} eV/K. The case of the E_0 temperature dependence is treated in the article by G. L. Hansen, J. L. Schmidt & T. N. Casselman, "Energy gap versus alloy composition and temperature in $Hg_{1-x}Cd_xTe$," J. Appl. Phys. **53(10)**, 7099-7101, 1982. They give $E_0(x,T)$ for MCT where $x < 0.6$.

20. M. H. Herman, I. D. Ward, R. C. Bowman, D. D. Smith, S. C. Moss, N. Chand, "Observation of Impurities in GaAs by electron beam electroreflectance (EBER)," presented at the American Physical Society Meeting, 20-24 March, 1989

21. M. H. Herman, I. D. Ward, S. E. Buttrill, Jr., and G. L. Francke, "Characterization of III-V semiconductor structures using electron beam electroreflectance (EBER) spectroscopy," presented to the Materials Research Society Meeting, Boston, MA, 1988. To be published in the conference proceedings.

22. A. Dodabalapur, V. P. Kesan, D. P. Neikirk, B. Streetman, M. H. Herman and I. D. Ward, "Photoluminescence and electroreflectance characterization of modulation-doped quantum wells" to be presented at the Electronic Materials Conference, Cambridge, MA, June 21-23, 1989.

APPENDIX

Electron Beam Electroreflectance (EBER) Analysis of Single $Al_xGa_{1-x}As$/GaAsQuantum Wells

by

M. H. Herman, S. E. Butrill, Jr. and G. L. Francke
of CHARLES EVANS & ASSOCIATES

and

F. A. Chambers
of AMOCO Corporation

was orally presented at the 1988 Electronic Materials Conference Meeting in Boulder in June 1988. It has been submitted for publication in the Journal of Electronic Materials.

Electron Beam Electroreflectance (EBER) Analysis of Single $Al_xGa_{1-x}As/GaAs$ Quantum Wells

M. H. Herman, S. E. Buttrill, Jr. and G. L. Francke

Charles Evans & Associates, Redwood City, CA

and

F. A. Chambers

AMOCO Corporation, Naperville, IL

ABSTRACT

Using the technique of electron beam electroreflectance (EBER), we have obtained spectra of $Al_{0.31}Ga_{0.69}As/GaAs$ [100]-oriented single quantum wells. Well widths of 10, 25, 50, and 100 Å nominal thickness were studied. The EBER spectra were compared to the predictions of the simple rectangular well model for the Γ reciprocal lattice point, using effective masses within the well of $m_{hh} = 0.34m_0$, $m_{lh} = 0.094m_0$, and $m_e = 0.0665m_0$. Differences between experimental and theoretical excitonic transition energies were minimized by adjustment of the well width and conduction band offset parameter Q_c, resulting in well widths within 15% of their nominal values and Q_c values between 0.61 and 0.65. In general, we find that spectra contain allowed ($\Delta n = 0$) and forbidden ($\Delta n \neq 0$) transitions between bound states.

Additionally, we consistently observe features which we ascribe to transitions between bound and delocalized "unconfined" or "resonant" states lying close to the AlGaAs band edge energies. These states are most evident in the thin wells, as the wider 50Å and 100Å wells contain many bound state transitions which mask the resonant levels. In particular, for the 10Å well we observe allowed transitions C1H1 and C1L1, and a third transition. The latter feature corresponds closely to a transition between H1 and the top of the conduction band well (CT), and to a transition between the bottom of the valence band well (VB) and C1. Likewise for the 25Å well, we observe allowed transitions C1H1 and C1L1, and distinct transitions between the top of the conduction band well and both H1 and L1.

From our 100Å EBER spectra, we observe a feature which may be due to quantum confinement at $E_0+\Delta_0$. In spectra of this sample, we note a feature lying slightly above the GaAs $E_0+\Delta_0$ energy, and which possesses a much larger intensity and uncharacteristic lineshape than observed for the interband $E_0+\Delta_0$ transition in bulk GaAs. This feature is suggestive of a transition between the C1 level and the lowest confined state of the split-off band.

I. INTRODUCTION

Both the theoretical understanding and experimental realization of solid state quantum wells have been well established [1]. Experimental observations of optical transitions in such structures have provided the impetus for advanced understanding of excitonic and interband transitions in confined systems [2]. In such studies, direct evidence of forbidden transitions and the evidence of unconfined or resonant states in single and multiple QW structures has come from modulation spectroscopies such as electroreflectance [3] (ER).

Recently, an ER system employing an electron beam for surface field modulation has been described [4]. The electron beam electroreflectance (EBER) instrument amplifies the magnitude of the surface potential by flooding the surface with low energy (~240eV) electrons. Owing to the square law dependence of the amplitude of ER signals upon the strength of the electric field modulation [5], EBER generally possesses higher signal-to-noise than alternative contactless modulated reflectance techniques such as photoreflectance.

The EBER technique probes all of the levels of the quantum well. EBER is one of several forms of electroreflectance (ER) modulation spectroscopy which have demonstrated superiority for such studies. The measure of the modulated reflected light intensity provides information at all energies, in comparison to PL, which only provides information about radiative recombination of the lowest transition energies. In ER, one measures as a function of light wavelength λ both the reflected light intensity, $R(\lambda)$, and its changes, $\Delta R(\lambda)$, which result from modulation of an electric field within the crystal. The ratio of the two, $\Delta R/R$, is a signal which reveals the optical transitions of the crystal.

In this paper, we describe applications of the EBER instrument to analysis of GaAs quantum wells bounded by $Al_xGa_{1-x}As$ barriers. Experimental EBER data from several such wells are presented. The observed lineshapes are characterized and quantified using established theory. The resultant energies are related to the parameters of the rectangular barrier model for the Γ point, using accepted effective mass values. Finally, the conduction band offset parameter, Q_c, is estimated, and our results compared to those of other researchers.

II. THEORY

The GaAs/AlGaAs quantum well (QW) has been successfully modeled in the past using a simple rectangular barrier. In this model, the QW is composed of symmetric energy "barriers" encasing a narrow band gap "well," as shown schematically in Figure 1. As indicated, the well has a conceptual width W and band gap E_{gW}. Both $Al_xGa_{1-x}As$ barrier layers have an identical band gap E_{gB}. The total energy available for carrier confinement, $\Delta E_g=(E_{gB}-E_{gW})$, is shared between the conduction and valence bands. The fraction available for conduction band confinement is designated the conduction band offset parameter, Q_c. It is further assumed that Q_c depends only upon the well and barrier materials, and not upon well width, temperature, or AlGaAs composition.

Based upon the rectangular barrier model, the Schrodinger equation provides us with a trancendental equation for the bound state energies [6]. The equation is solved numerically for various well widths, depths, and effective mass values appropriate to each subband, consistent with a range of Q_c values. The general behavior of the bound states as a function of well depth have been described [7]. From the bound state energies of each subband, inter-subband transitions can be calculated. In Figure 1, we have labelled the conduction band states C*n* for the nth level above the bottom of the well. Similarly, L*n* and H*n* refer to the light and heavy hole levels of the valence band.

In the present case, we must also consider the possibility that transition between conduction band levels and quantized states associated with the split-off valence band may be observable. Quantum confinement has already been reported by others at the E_1 band gap [8], and excitons have been observed at the $E_0+\Delta_0$ band gap in the past [9]. In bulk GaAs, the splitoff valence band lies approximately 0.33 eV below the degenerate light and heavy hole valence maxima at Γ. As the effective mass of this valence band is nearly 0.15, the lowest quantum transition (C1S1) of this split-off band well is therefore be predicted to lie about 0.33 eV above the C1H1 transition.

Based upon earlier research [10], we expect the QW to also possess unbound (unconfined, resonant) states outside of the conduction and valence band wells. These states are predicted theoretically by more sophisticated models [11]. For simplicity, we have conceptually grouped these additional levels under the labels CT for "conduction band *top*" and VB for "valence band *bottom*." The bound and unbound levels of the QW are the solutions of the Schrodinger equation, with effective mass parameters representative of the crystalline solid. Although the effective masses may possess a slight temperature dependence, we will use the constant values suggested recently by Shanabrook, *et al* [12]. Specifically, we use $m_e = 0.067$, $m_{hh} = 0.34$, $m_{lh} = 0.094$ for the electron, heavy hole, and light hole masses in the (100) direction, in units of the free electron mass. The energy levels of these unbound states are also depicted schematically in Figure 1.

III. EXPERIMENTAL:

The QW samples were grown by MBE at AMOCO. An initial GaAs epi layer prefaced the growth of the QW layers. The thicknesses and nominal *x* values of the barriers and well are indicated in Table 1. Neither GaAs capping layers nor intentional dopants were used in the preparation of these samples, to alleviate possible effects which may arise from carrier confinement in the cap or from large built-in electric fields due to doping.

The EBER measurements were carried out near 90K or 300K, and monitored by means of an Fe-Constantan thermocouple. During analysis, samples were maintained under pressures of 10^{-9} torr. Electron beam currents on the order of 1 μA or less, focussed to an 0.8 mm diameter spot, were employed to provide a suitably strong modulation. At the sample surface, the electrons retained 240 eV of kinetic energy, which thermalize within 25 Å of the surface [13].

The probe light beam was provided by a 0.25 meter PTI Model 1 monochromator, employing a 1200 line/mm grating. The monochromator was illuminated by a 75 Watt Xe arc lamp. The monochromator wavelength was stepped by an IBM PC/AT computer, and the signal acquired successively at each wavelength step. The reflected probe light was detected with a Si photodiode. The photocurrent signal was separated into AC and DC components electronically, and measured by an EG&G PAR model 5207 lockin amplifier synchronized to the electron beam. The numerical division of the two signals provided the measured $\Delta R/R$ EBER spectrum.

We have analyzed the EBER spectra by non-linear least-squares fitting of the experimental data to a superposition of Lorentzian lineshapes [14], representing independent transitions. These individual transitions may have an interband, excitonic, or impurity-to-band origin, which may be modeled by appropriate choices of derivative and dimensionality. Presently, we have incorporated the Marquardt algorithm for automated variation of the broadening parameter Γ, the transition energy E, and the dimensionless quantities of amplitude and phase factor. We are interested mainly in the comparison between the experimental energies to those predicted by the model, so that the parameters Q_c and W can be deduced.

We have not treated impurities in this study. Impurities can cause bound excitons as well as impurity-to-band transitions, which can each give features in modulated reflectance spectra. Although infrequently such impurity signatures have been observed below the GaAs E_0 at some positions on these QW samples (see Figure 3 for example), the QW transitions have been found to be unchanged at locations where impurities have not been observed. We therefore consider the effects of impurities in the case of these QW samples to be inconsequential, while remaining cognizant of this assumption.

IV. EXPERIMENTAL RESULTS AND DISCUSSION:

An EBER spectrum of MBE grown AlGaAs on GaAs is shown in Figure 2. This spectrum shows the energies and typical magnitudes of the GaAs and AlGaAs E_0 transitions at 95K. It shows the EBER spectrum of an AlGaAs film on GaAs to be free of observable transitions between the AlGaAs and GaAs E_0 band gaps [15]. We can observe the GaAs $E_0+\Delta_0$ transition 0.33 eV above the E_0 transition. However, the intensity of the split-off band transition is usually quite weak relative to the E_0 transitions [16].

For comparison to Figure 2, the experimental EBER data for the 10, 25, 50 and 100Å quantum wells are shown respectively in Figures 3, 5, 7, and 9. The spectra are expanded in various energy ranges to show the resolvable transitions. In each case, we observe excitonic lineshapes within the energy range between the GaAs and AlGaAs E_0 band gap energies, in agreement with previous reports [17]. We have annotated the spectra with tentative designations of the most intense features, based upon the rectangular barrier model. The determination of the transition assignments is discussed below.

Several effects influence the measured transition energies and intensities. Although only transitions from states of identical symmetry may be expected from a perfectly symmetric QW, in practice we observe transitions between states of opposite symmetry as well. These transitions are a consequence of asymmetries resulting from built-in and applied electric fields. Electric field modulation causes both the energy levels and wavefunctions to be Stark shifted within the well. These effects change the wavefunction overlap and thereby affect absorption and reflection of light by the structure, providing the measured modulated reflectance signal.

Accordingly, built-in fields may also introduce Stark-effect perturbations of unmodulated electronic levels, introducing uncertainties in the comparison of experimental to theoretical results [18]. Indeed, we have observed that the C1H1 and C1L1 transitions are composed of distinct excitonic doublets of opposite phase. In the case of the 50 Å spectrum, we find the energy change to be about 4.5 meV for the C1H1 level, and 8.3 meV for the C1L1 level. However, these energies only reflect the changes due to electron beam modulation, and do not indicate the effects of built-in electric fields. In spite of these issues, we compare below the experimental results to the rectangular barrier model disregarding possible Stark shifts of the levels.

I. THE 10 ANGSTROM WELL.

For the 10 Å well shown in Figure 3, only three distinguishable transitions are observed. All three lie below the AlGaAs E_0, and close to the expected GaAs $E_0+\Delta_0$ split-off band. The proximity of the QW transitions to the substrate GaAs $E_0+\Delta_0$ and barrier AlGaAs E_0 levels places some uncertainties on their origin due to possible impurity-related or interference effects. However, our examinations of the transition energies, broadening parameters, and lineshapes show that the observed levels do not coincide with the GaAs $E_0+\Delta_0$ level, nor to impurity transition features we have observed in bulk GaAs, even though we do observe an impurity feature 39 meV below the GaAs E_0 transition in this sample, as noted in Figure 3. Therefore, we assign the features below the AlGaAs E_0 to excitonic transitions of the QW.

The experimental EBER data taken at 298K, shown in Figure 3, and data taken at 103K show two strong peaks separated by nearly 0.02 eV, and lying about 0.07eV below the AlGaAs E_0 level. Theoretically, this well may possess only C1, L1, and H1 bound states, so we take these two features to be the C1H1 and C1L1 transitions. Using the adjustable parameters are the well width W, and the band offset Q_c, we have minimized the squared differences between the theoretical and experimental levels, weighted by the experimentally estimated broadening parameter. The results of the minimization procedure appear in Table 2. The procedure gives an extimated well width of 11.57 Å and a Q_c of 0.644. A spectrum of the same sample taken at 103K is best modeled by a similar well width of 11.62 Å and Q_c of 0.646.

We also observe in the experimental data additional transitions below the AlGaAs E_0 level, which do not correspond to any transitions between bound states of this well. The levels do correspond closely to transitions between the bound levels and the resonant states at the top and bottom of the GaAs wells, CT and VB. The experimental and theoretical levels are compared graphically in Figure 4.

II. THE 25 ANGSTROM WELL

An EBER spectrum of the 25 Å well appears in Figure 5, with several observable transitions. The 25 Å well contains C1, L1 and H1 bound levels, and as in the case of the 10 Å well, resonant states CT and VB are also proposed. None of the observed levels coincide with the GaAs $E_0+\Delta_0$ level. The EBER spectra of the 25 Å QW data consistently show excitonic lineshapes with energies listed in Table 3. No impurity-related features are observed below the GaAs E_0.

The results of least squares minimization of the differences between theoretical and experimental levels appear in Table 2. The well width is estimated to be 25.9 Å and a Qc of 0.612. As in the case of the 10Å well, we observe additional experimental transitions below the AlGaAs E_0 level which do not correspond to bound state transitions in this well, but which do correspond to transitions between the bound levels and the resonant state. The experimental and theoretical levels are compared in Figure 6.

III. THE 50 ANGSTROM WELL

From the EBER spectrum of the 50 Å well, shown in Figure 7, many transitions are observed. Though a well which is 50 Å wide is predicted to contain C1, C2, L1, L2, H1, H2, and H3 bound levels, we find that the well is slightly narrower, and does not contain transitions to C2, L2, or H3 levels. Again, the GaAs $E_0+\Delta_0$ level is unobserved, and we propose resonant states CT and VB to explain additional features of the EBER spectrum.

As above, we have obtained W and Q_c by minimization of the weighted squared differences between the theoretical and experimental levels. The best results are obtained from a W of 42.86 Å and Q_c of 0.618, as summarized in Table 4 . As in the case of the thinner wells, we again observe additional experimental transitions which do not correspond to transitions between two bound states, but instead are ascribed to transitions between bound and resonant states. The experimental and theoretical levels are presented in Figure 8.

IV. THE 100 ANGSTROM WELL

In the case of the 100 Å well shown in Figure 9, a large number of transitions are observed. The 100 Å well is predicted to contain C1-C3, L1-L3, and H1-H5 bound levels. Based upon the observations in the thinner wells, we anticipate the existence of resonant states CT and VB. The well width W and Q_c are determined as above. The results appear in Table 5 which shows a well width of 101.0 Å and Q_c of 0.639. Additional experimental levels which correspond to transitions between the bound levels and the resonant states are suggested, but are often masked by bound transitions. The experimental and theoretical levels appear graphically in Figure 10.

From our 100Å EBER spectra, we observe a feature which may be due to quantum confinement at $E_0+\Delta_0$. In spectra of this sample, we note a feature at 1.898 eV, lying slightly above the GaAs $E_0+\Delta_0$ energy of 1.834 eV, and which possesses a much larger intensity and uncharacteristic lineshape than observed for the interband $E_0+\Delta_0$ transition in bulk GaAs. The levels which surround this feature are the C3L3 and C3VB transitions. However, the observed feature is much more intense than the C2L2 or C2VB levels from this sample. Therefore, this feature is suggestive of a transition between the C1 level and the lowest confined state of the split-off band. As the split-off band effective mass is intermediate between that of the light or heavy holes, the transition between the 1st conduction band level C1 and the first split-off band level S1 should lie about 0.34 eV above the C1H1 to C1L1 levels. In the thinner wells, the C1S1 level would be above the AlGaAs E_0 level, and therefore be attenuated in intensity. In the case of the 100 Å QW, this level lies below the AlGaAs E_0. Supplementary features observed above the AlGaAs E_0 transition in all samples may have similar origins, but may also be related to Franz-Keldysh effects, which mask their clear determination.

V. CONCLUSION:

In this paper, we have presented experimental Electron Beam Electroreflectance (EBER) spectra from four AlGaAs/GaAs/AlGaAs quantum wells. We demonstrated that the observed optical transitions from quantum wells can be successfully understood on the basis of the rectangular barrier model. The transitions present in the experimental EBER data were fitted to excitonic lineshapes. The resulting transition energies were then compared to the theory, and optimized by variation of the W and Q_c parameters. For each of the wells, reasonable assignments have been made on the basis of peak intensity.

Additionally, we have confirmed the observation of forbidden but parity allowed $\Delta N = 0$ transitions in many cases [19]. Further, parity forbidden transitions such as C1H2 and C2H1 are also observed clearly in some samples. These transitions are understood to occur from electric field modulation of square QWs [20]. Additional peaks are experimentally observed, which suggest transitions to unconfined or resonant states lying outside the well. These features and their assignments are most evident in the thinnest wells, where they are not masked by bound state transitions. In the case of the 100 Å QW, we find a large feature at the energy predicted for a transition between C1 and S1, the lowest level of the splitoff valence band of the GaAs well. The absence of alternatively strong transitions at this energy suggests that the level is C1S1.

Further, we have obtained estimates of the parameters W and Q_c for each well. These results are summarized in Table 6. In all cases, the well widths are calculated to be within 15% of their nominal values. The Q_c estimates lie within the range of 0.612 to 0.646. The average of 0.629 is in close agreement with values quoted by others using the effective mass values we have adopted [21]. Other choices of effective mass affect the calculated Q_c value, and do not represent valid comparisons, although the agreement between experiment and theory may be quite similar. This interaction between Q_c and effective mass choices have resulted in many combinations of values [22]. Wolford [23] used pressure to determine the crossing of the bands and found an independent measure of Q_c to be 0.685. If this value Q_c is correct, it suggests that the effective mass values may be incorrect. Reddy *et al* found $Q_c = 0.65$ with $m_{hh} = 0.45$, and attributed observed structures above E_0 of $Al_xGa_{1-x}As$ to resonant (unconfined) transitions. Their data was fitted with lineshapes appropriate to interband transitions, and not excitonic lineshapes for their observed features. However, the choice of lineshape should not have introduced significant errors in estimation of transition energies.

VI. ACKNOWLEDGEMENTS:

The authors have enjoyed beneficial interactions with many individuals. Professor P. Raccah of the University of Illinois at Chicago provided stimulating discussions about these quantum wells, based upon his work with AlGaAs/GaAs superlattices [24], and suggested the analysis of these samples by EBER. Young De of the University of Illinois at Chicago helped with acquiring some of the spectra presented here. We also are pleased to acknowledge Professor F. Pollak of the Institute of Applied Sciences, Brooklyn College of CUNY for his suggestions, and Dr. B. V. Shanabrook of the Naval Research Lab who kindly provided us with preprints of recent work. We thank S. Sputz of AT&T Bell Labs for suggesting the possibility of transitions related to the GaAs splitoff band in the 100 Å QW.

This work was supported in part by the Army and Defense Advanced Research Projects Agency under contract DAAH01-88-C-0873, and by the Office of Naval Research under contract N00014-88-C-0221.

VII. REFERENCES:

1 For a review of QW theory, see for example W. T. Masselink, P. J. Pearah, J. Klem, C. K. Peng, H. Morkoc, G. D. Sanders & Y.-C. Chang, Phys. Rev. B32(12), 8027 (1985).

2 See for example C. Weisbuch, Semiconductors and Semimetals, Chapter 1, vol 24, R. Dingle, R. K. Willardson and A. C. Beer, eds. 1972.

3 U. K. Reddy, G. Ji, T. Henderson, H. Morkoc & J. N. Schulman, J. Appl. Phys. **62**(1), 145 (1987). O. J. Glembocki, B. V. Shanabrook, N. Bottka, W. T. Beard, and J. Comas, Appl. Phys. Lett. **46**(10), 970 (1985).

4 P. M. Raccah, J. W. Garland, S. E. Buttrill, Jr., L. Franke & J. Jackson, Appl. Phys. Lett. **52**(19) 1584 (1988). Recent studies at our laboratory suggest that the major effect of the low current density electron beam is to charge the surface, as suggested by I. Broser, R.-A. Hoffman & H.-J. Schulz, Solid State Comm. **8** 587 (1970).

5 For the excitonic case, see D. F. Blossey & P. Handler, Semiconductors and Semimetals, Chapter 3, vol 9, R. K. Willardson and A. C. Beer, eds. 1972. For the interband case, see D. E. Aspnes, Surface Science **37** pp. 418 (1973).

6 W. T. Masselink, P. J. Pearah, J. Klem, C. K. Peng, H. Morkoc, G. D. Sanders & Y.-C. Chang, Phys. Rev. **B32**(12), 8027 (1985).

7 See for example R. C. Miller, D. A. Kleinman & A. C. Gossard, Phys. Rev. B29(12) 7085 (1984).

8 R. P. Vasquez, R. T. Kuroda, & A. Madhukar, J. Appl. Phys. **61**(8), 2973 (1987). See also M. Erman, J. B. Theeten, P. Frijlink, S. Gaillard, Fan Jia Hia, & C. Alibert, J. Appl. Phys. **56**(11), pp. 3241 (1984).

9 D. E. Aspnes & A. A. Studna, Surface Sci. **37**, 631 (1973).

10 U. K. Reddy, G. Ji, T. Henderson, H. Morkoc & J. N. Schulman, J. Appl. Phys. **62**(1), 145 (1987).

11 The envelope function method is described by G. Bastard, U. O. Ziemelis, C. Delalande, M. Voos, A. C. Gossard & W. Wiegmann, Solid State Comm. **49**(7), 1038 (1984). Tight-binding calculations have been described by J. N. Schulman & Y.-C. Chang, Phys. Rev. **B31**(4) 2056 (1985).

12 Effective masses for GaAs have been recently given by B. V. Shanabrook, O. J. Glembocki, D. A. Broido & W. I. Wang, Phys. Rev. **B39**(5), 3411, 1989.

13 From Monte Carlo simulations, 250eV electrons penetrate no more than 20Å into GaAs. The mean free path is 33Å, but substantial scattering stops them within 10Å of the surface; the backscattering coefficient is about 0.3. For AlAs, the backscattering coefficient only about 0.15, and the mean free path is about 40Å.

14 For a discussion of interband lineshapes, see J. W. Garland, & P. M. Raccah, SPIE **659**, 32, Materials Technologies for IR Detectors (1986). The effects of impurities has been discussed by B. V. Shanabrook, Surface Sci. **170**, 449 (1986).

15 We must make note that interference effects and impurity-related features in such films can be observed. However, the energy spacings of interference-related features in ER spectra are relatively constant, of consistent amplitude, and predictable periodicity. Further, we find interference effects to be generally less severe in MBE films than in MOCVD grown films. Impurity effects pose a more fundamental problem which one must treat as a possibility. However, only impurity-bound excitons, lying close to the AlGaAs E_0, should have a lineshape commensurate with the transitions originating within the QW.

16 The E_0 transition appears more intense and sharp than $E_0+\Delta_0$ only because of the influence of excitons at E_0. The authors find that in samples which have been implanted and annealed, the two features have similar widths and intensities.

17 X. L. Zheng, D. Heiman, B. Lax, F. A. Chambers & K. A. Stair, Appl. Phys. Lett. **52**(12) 984 (1988).

18 W. Potz & D. K. Ferry, Phys. Rev. **B32**(6) 3863 (1985).

19 C. Weisbuch, R. C. Miller, R. Dingle, A. C. Gossard, & W. Wiegmann, Solid State Comm., **37**, 219 (1981).

20 W. Potz & D. K. Ferry, Phys. Rev. **B32**(6) 3863 (1985).

21 O. J. Glembocki, B. V. Shanabrook, N. Bottka, W. T. Beard, and J. Comas, Appl. Phys. Lett. **46**(10), 970 (1985).

22 A listing follows with the first author, year, and the combinations (m_{hh},m_{lh},Q_c): R. Dingle *et al* Phys. Rev. Lett. **33**(14), 827 (1974): (0.45,0.08,0.88); R. C. Miller *et al* Phys. Rev. B29(12) 7085 (1984): (0.34,0.094,0.57); O. J. Glembocki *et al* Appl. Phys. Lett. **46**(10), 970 (1985): (0.34,0.094,0.60); Erman *et al* J. Appl. Phys. **56**(11), 3241 (1984): (0.48,0.087,-) and J. Appl. Phys. **63**(2), 465 (1988): (0.62,0.087,0.6); and Reddy *et al* J. Appl. Phys. **62**(1), 145 (1987): (0.45,-,-). The (-) signifies that the parameter was not specified in the paper.

23 D. J. Wolford, T. F. Kuech, J. A. Bradley, M. A. Gell, D. Ninno, & M. Jaros, J. Vac. Sci & Technol. **B4**(4), 1043 (1986).

24 P. M. Raccah, J. W. Garland, Z. Zhang, F. A. Chambers & D. J. Vezzetti, Phys. Rev. **B36**, 4271 (1987).

VIII. FIGURES AND CAPTIONS:

I Figure 1: Rectangular barrier model:

Figure 1: Schematic of QW, showing large band gap Barrier surrounding narrow gap Well material. States of the well are schematically indicated: conduction band states C*n*, light hole levels L*n* and heavy hole levels H*n*. Not shown is the split-off valence band, which lies 0.34 eV (Δ_0) below the degenerate light and heavy hole valence maxima. The states of this split-off band well are similarly labeled S*n* in the text. Unconfined transitions VB and CT refer to the valence band bottom and conduction band top, respectively.

II. Figure 2: EBER spectrum of AlGaAs film on GaAs.

The EBER spectrum of a single AlGaAs film on GaAs. We can also observe the GaAs $E_0+\Delta_0$ transition 0.342 eV above the E_0 transition.

III. Figure 3: EBER spectrum of 10A QW.

EBER spectrum of 10Å QW at 298K shows GaAs substrate E_0 at 1.424eV, AlGaAs E_0 at 1.855eV, and transitions just below AlGaAs E_0 due to GaAs QW. The energy regime just below the AlGaAs E_0 has been expanded to show the structure of the QW transitions. Three transitions are observed distinctly separated from the AlGaAs E_0, labelled with calculated assignments. An impurity related transition is also observed 39 meV below the GaAs E_0 transition.

IV. Figure 4: Comparison of Theoretical to Experimental Assignments for 10A QW.

The correspondence between the rectangular barrier model transitions and experimentally determined energies from EBER are shown. The final Q_c is 0.646, and well width 11.62 Å.

V. Figure 5: EBER spectrum of 25A QW.

EBER spectrum of 25Å QW at 90K shows GaAs substrate E_0 at 1.505eV, AlGaAs E_0 at 1.91eV, and transitions between due to GaAs QW levels. The energy regime just below the AlGaAs E_0 has been expanded to show the structure of the QW transitions. In addition to the C1H1 and C1L1, three transitions are observed distinctly separated from the AlGaAs E_0 are attributed to transitions between bound and unbound levels.

VI. Figure 6: Comparison of Theoretical to Experimental Assignments for 25A QW.

The correspondence between the rectangular barrier model transitions and experimentally determined energies from EBER are shown. The final Q_c is 0.612, and well width 25.90 Å.

VII. Figure 7: EBER spectrum of 50A QW.

EBER spectrum of 50Å QW at 90K shows GaAs substrate E_0 at 1.505eV, AlGaAs E_0 at 1.91eV, and transitions due to GaAs QW levels between these. The spectrum has been expanded to show the weaker QW transitions, which have been labelled with calculated assignments.

VIII. Figure 8: Comparison of Theoretical to Experimental Assignments for 50A QW.

The correspondence between the rectangular barrier model transitions and experimentally determined energies from EBER are shown. The final Q_c is 0.618, and well width 42.86 Å.

IX. Figure 9: EBER spectrum of 100A QW.

EBER spectrum of 100Å QW at 90K. Transitions due to GaAs QW levels appear in the expanded spectrum, with assignments based upon the rectangular barrier model. Strong transitions Note the large transition at 1.85eV, which may be due to transitions between C1 and the lowest splitoff valence band level S1.

X. Figure 10: Comparison of Theoretical to Experimental Assignments for 100A QW.

The correspondence between the rectangular barrier model transitions and experimentally determined energies from EBER are shown. The final Q_c is 0.639, and well width 101.0 Å.

Table 1: Nominal well and barrier thicknesses for QW samples.

Sample Number	Lower Barrier $Al_{0.3}Ga_{0.7}As$ thickness (Å)	Well GaAs thickness (Å)	Upper Barrier $Al_{0.3}Ga_{0.7}As$ thickness (Å)
249	5500	10	1000
250	4160	25	1000
251	5000	50	1000
252	1600	100	1000

Table 2: Best fit values for 10 Å Quantum Well.

Temperature	103K	298K
Qc	0.646	0.644
Well Width	11.62	11.57

Temperature	103K	103K	298K	298K
Transition Designation	Experimentally Observed Energy (eV)	Predicted Transition Energy (eV)	Experimentally Observed Energy (eV)	Predicted Transition Energy (eV)
GaAs	1.505	1.505	1.424	1.424
C1H1	1.842	1.842	1.770	1.769
C1L1	1.860	1.867	1.792	1.793
C1VB	1.889	1.883	1.814	1.810
CTH1	1.889	1.884	1.814	1.811
CTL1	1.907	1.909	1.833	1.835
AlGaAs	1.907	1.905	1.855	1.824

Table 3: Best fit values for 25 Å Quantum Well at 85K.

Temperature	85
Q_c	0.612
Well Width (Å)	25.90

Transition Designation	Experimentally Observed Energy (eV)	Predicted Transition Energy (eV)
GaAs	1.5050	1.5050
C1H1	1.7058	1.7058
C1L1	1.7321	1.7450
C1VB	1.8126	1.8128
CTH1	1.8382	1.8218
CTL1	1.8487	1.8610
AlGaAs	1.9000	1.9050

Table 4: Best fit values for 50 Å Quantum Well at 90K.

Temperature	90
Q_c	0.618
Well Width (Å)	42.86

Transition Designation	Experimentally Observed Energy (eV)	Predicted Transition Energy (eV)
GaAs	1.5050	1.5050
C1H1	1.6121	1.6162
C1L1	1.6405	1.6488
C1H2	1.7050	1.6958
C1VB	1.7479	1.7395
CTH1	1.7479	1.7659
CTL1	1.8148	1.7985
CTH2	1.8540	1.8455
AlGaAs	1.9050	1.9050

Table 5: Best fit values for 100 Å Quantum Well at 90K.

	Best fit for
Temperature	90
Q_c	0.6388
Well Width (Å)	101.03

Transition Designation	Experimentally Observed Energy (eV)	Predicted Transition Energy (eV)
GaAs	1.5083	1.5080
C1H1	1.5443	1.5458
C1L1	1.5570	1.5590
C1H2	1.5632	1.5687
C1H3	1.6070	1.6058
C1L2		1.6185
C2H1	1.6371	1.6340
C2L1	1.6371	1.6472
C1H4		1.6540
C2H2	1.6564	1.6570
C1L3	1.6801	1.6844
C1VB	1.6801	1.6863
C1H5		1.6880
C2H3		1.6941
C2L2	1.7058	1.7068
C2H4	1.7489	1.7423
C3H1	1.7549	1.7602

C2L3		1.7727
C3L1		1.7734
C2VB		1.7746
C2H5		1.7763
C3H2	1.7796	1.7832
CTL1		1.7844
CTH1	1.7796	1.7866
CTH2		1.7942
C3H3	1.8147	1.8203
CTH3		1.8313
C3L2		1.8330
CTL2	1.8566	1.8594
C3H4		1.8686
C1S1	1.8975	1.8864
C3H5		1.8892
CTH4		1.8949
C3L3	1.8975	1.8966
C3VB		1.9008
CTH5		1.9135
AlGaAs	1.9089	1.9080

Table 6: Summary of Calculated Well Thicknesses and Q_c Parameters.

Temperature(K)	103	298	85	90	90
Q_c	0.646	0.644	0.612	0.618	0.639
Nominal W(Å)	10	10	25	50	100
Calc W(Å)	11.62	11.57	25.90	42.86	101.03
% W dif	16.2	15.7	3.6	-14.3	1.0

Bound State Energies and Wavefunction Labels in Quantum Well

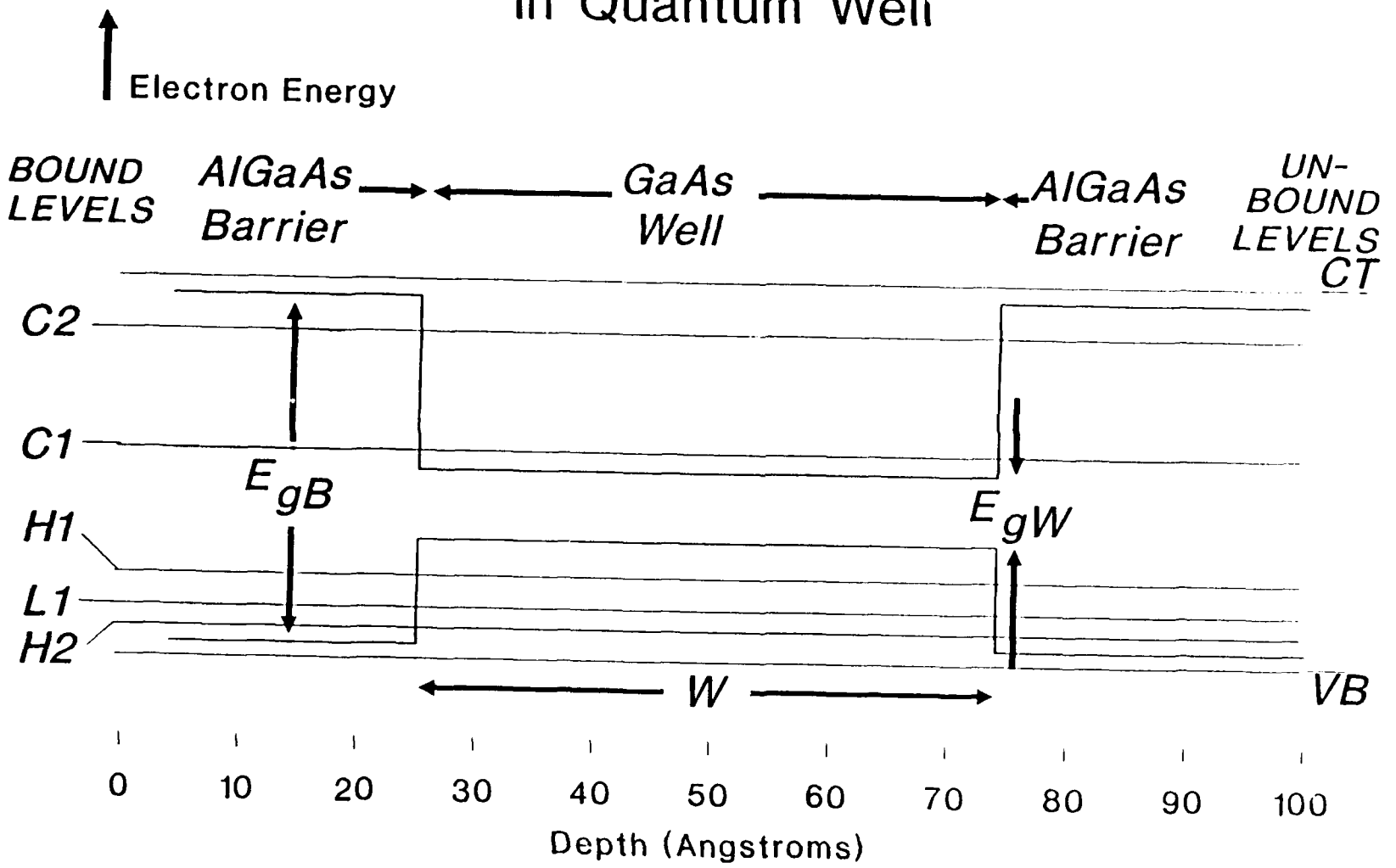

M. H. Herman, et al "Electron Beam Electroreflectance ..."
Figure 1

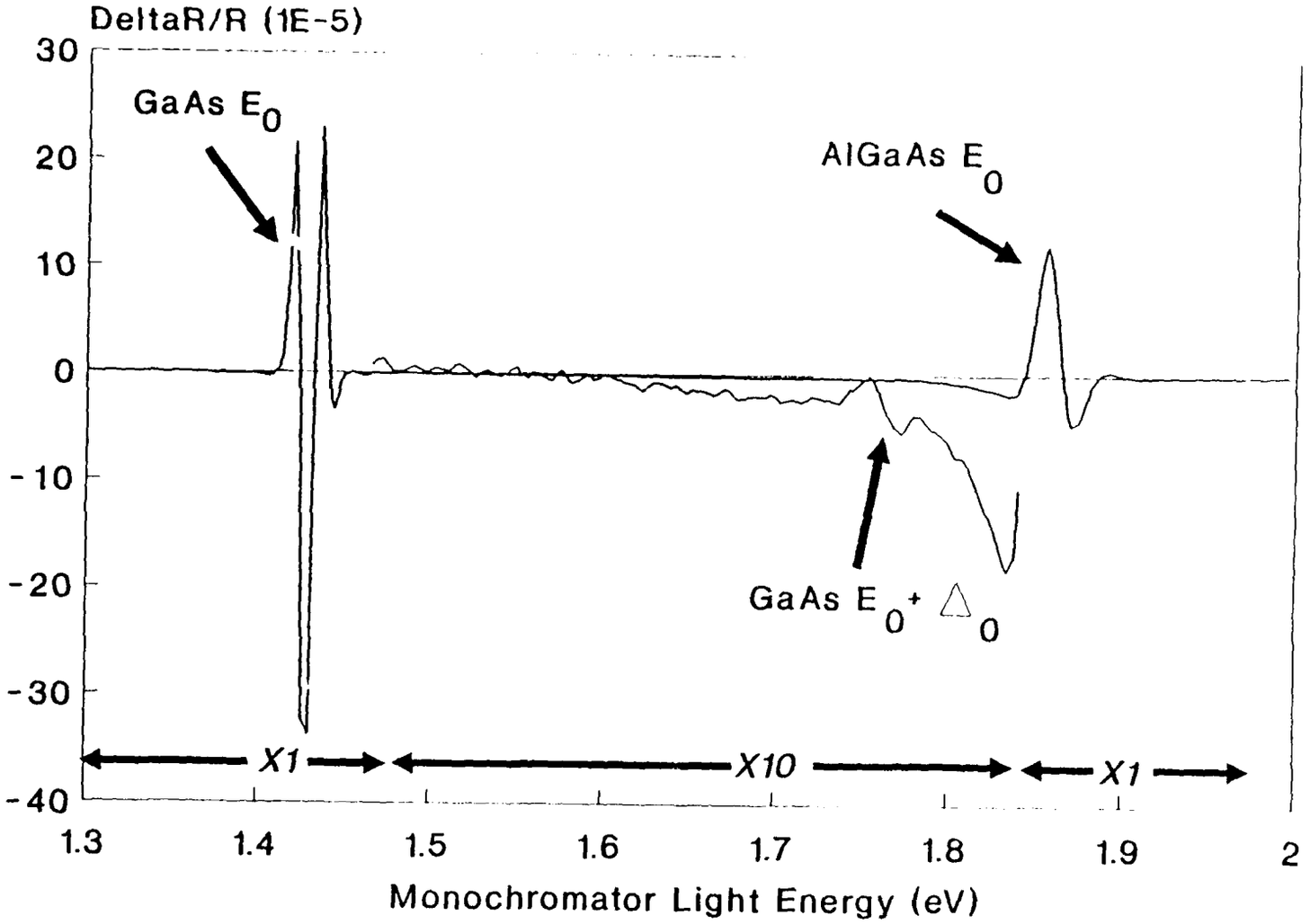

M. H. Herman, et al "Electron Beam Electroreflectance ..."
Figure 2

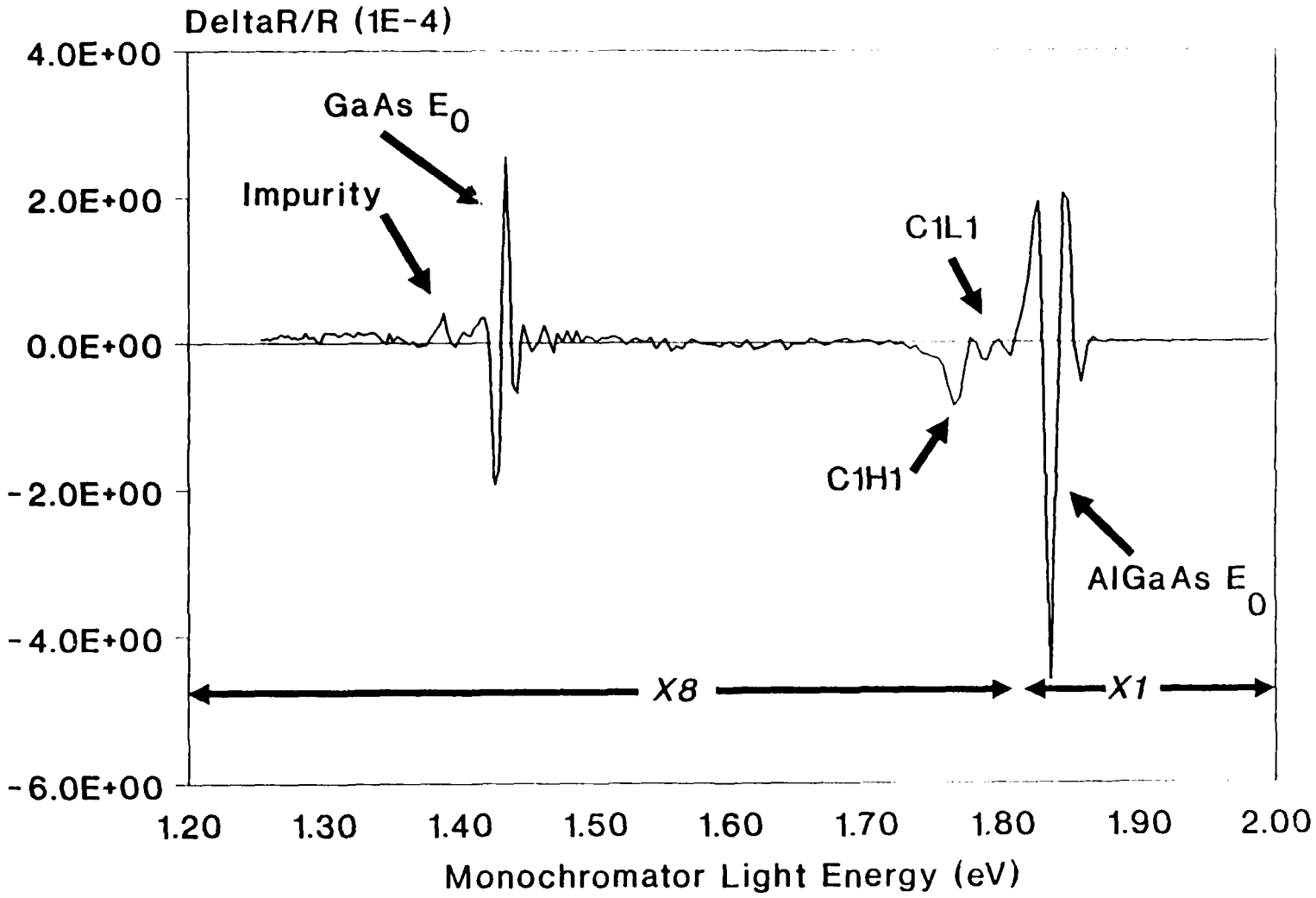

M. H. Herman, et al "Electron Beam Electroreflectance ..."
Figure 3

Best Fit to 10A Single Quantum Well
Qc=0.646, Width = 11.62, Depth = 0.4eV

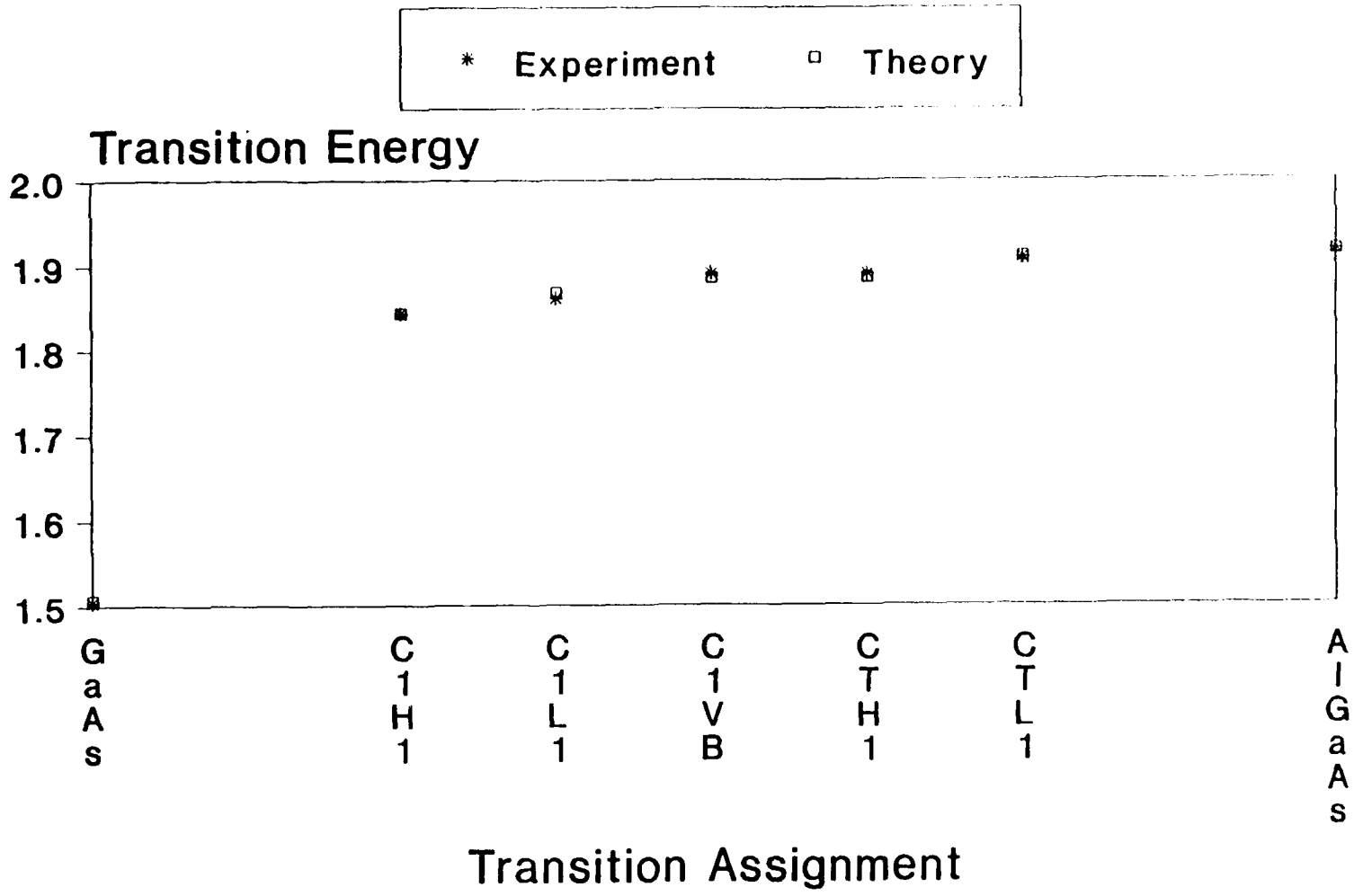

M. H. Herman, et al "Electron Beam Electroreflectance ..."
Figure 4

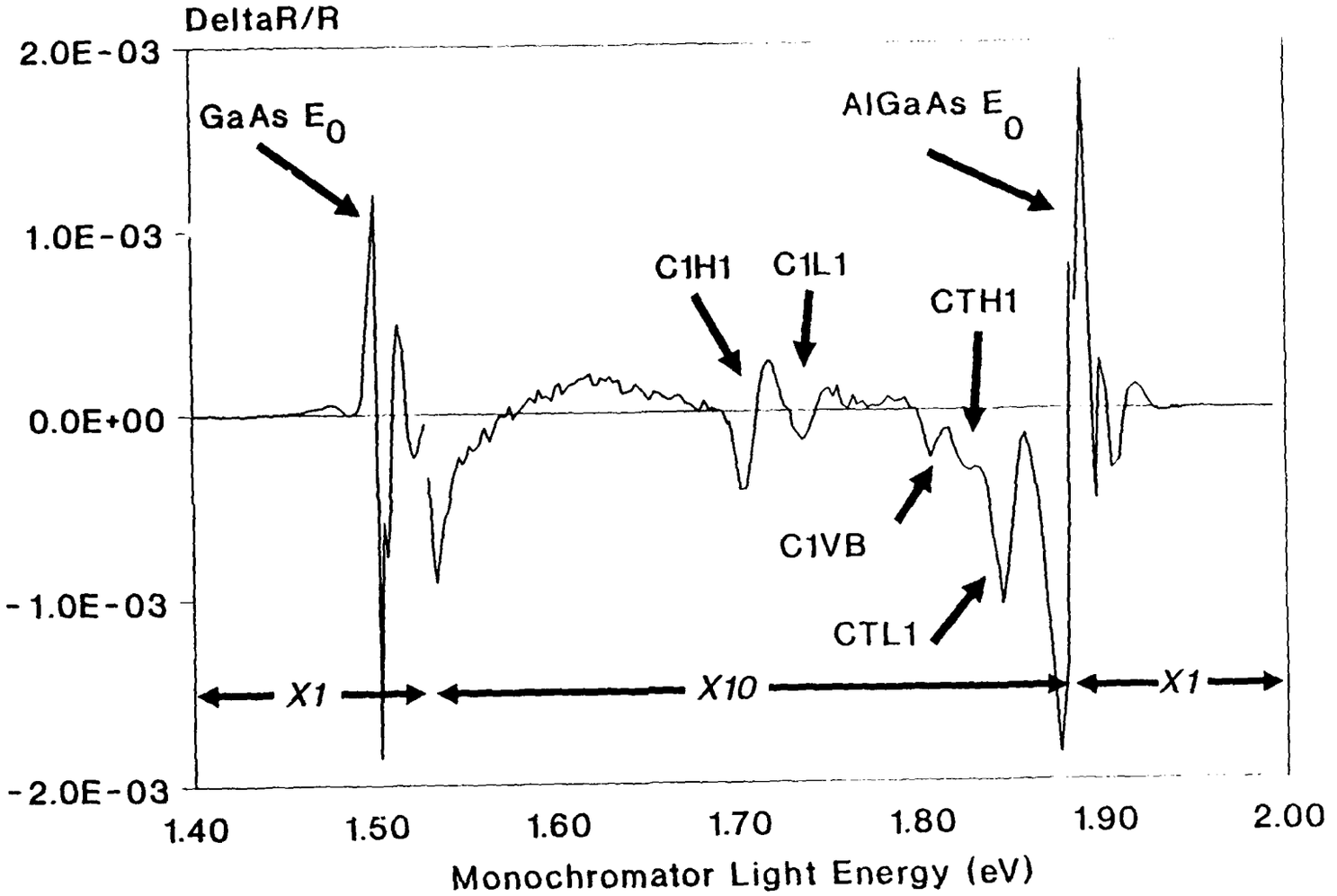

M. H. Herman, et al "Electron Beam Electroreflectance ..."
Figure 5

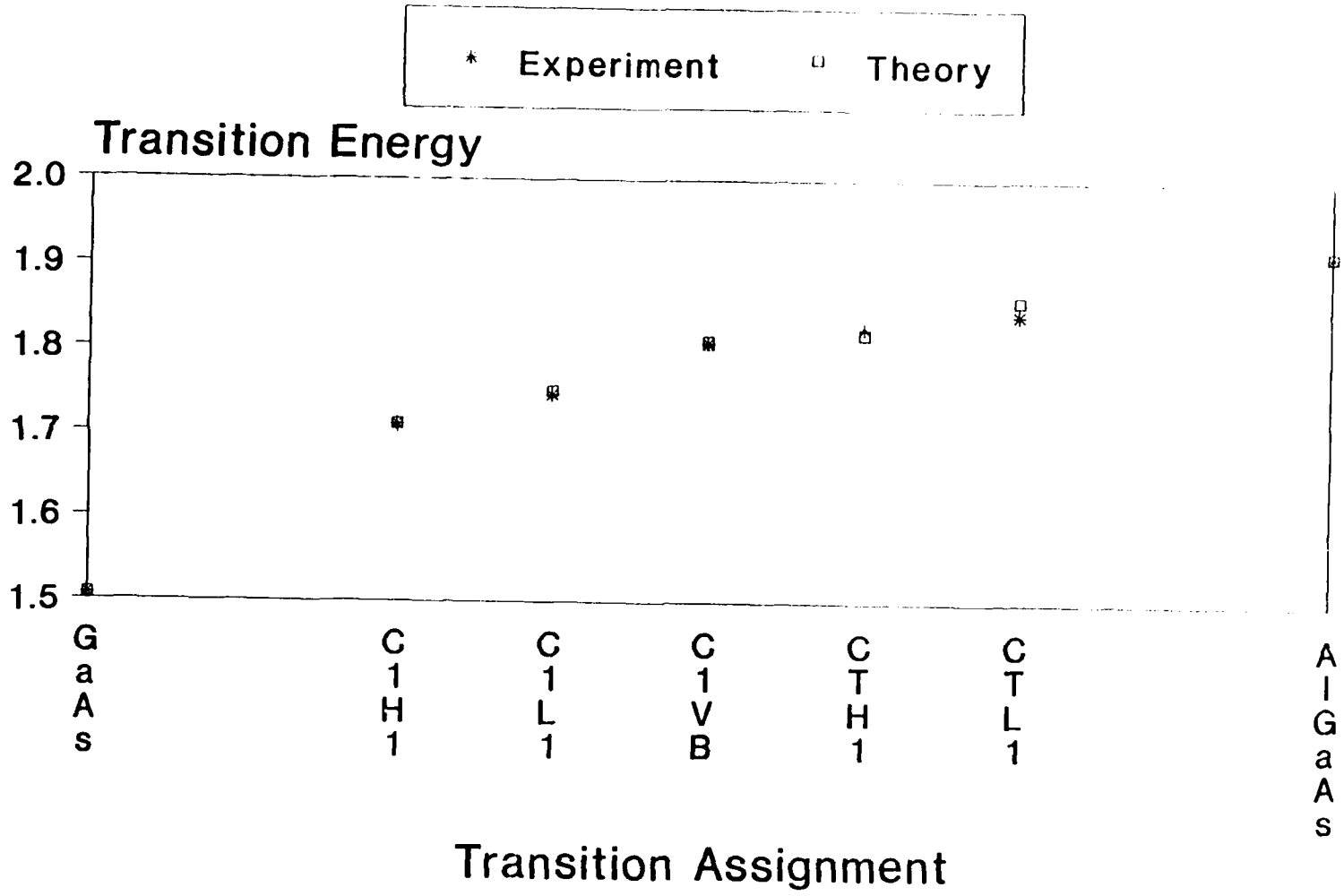

M. H. Herman, et al "Electron Beam Electroreflectance ...
Figure 6

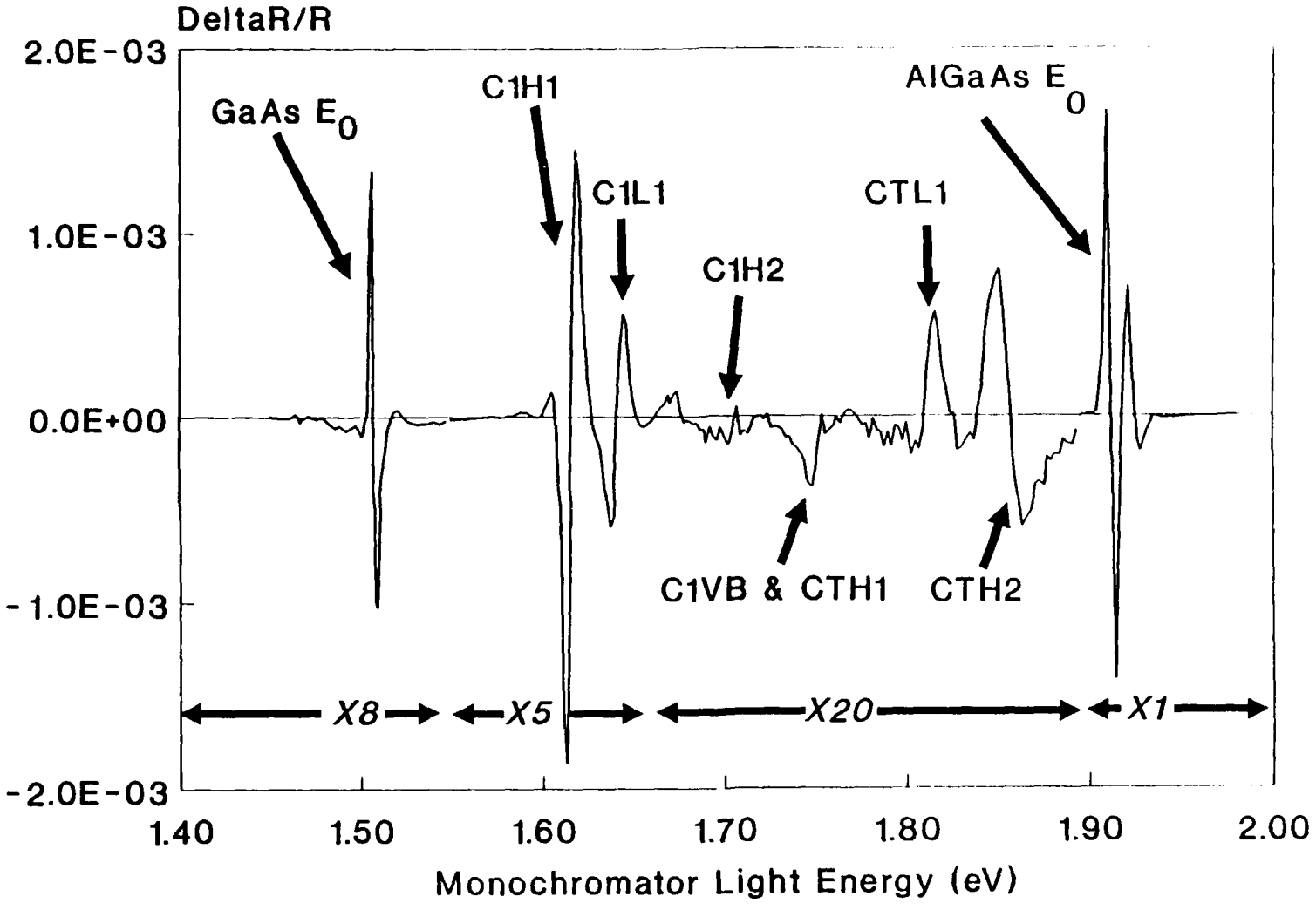

M. H. Herman, et al "Electron Beam Electroreflectance ..."
Figure 7

Best Fit to 50A Single Quantum Well
Width=42.9 A, Qc=0.618, Depth=0.4eV

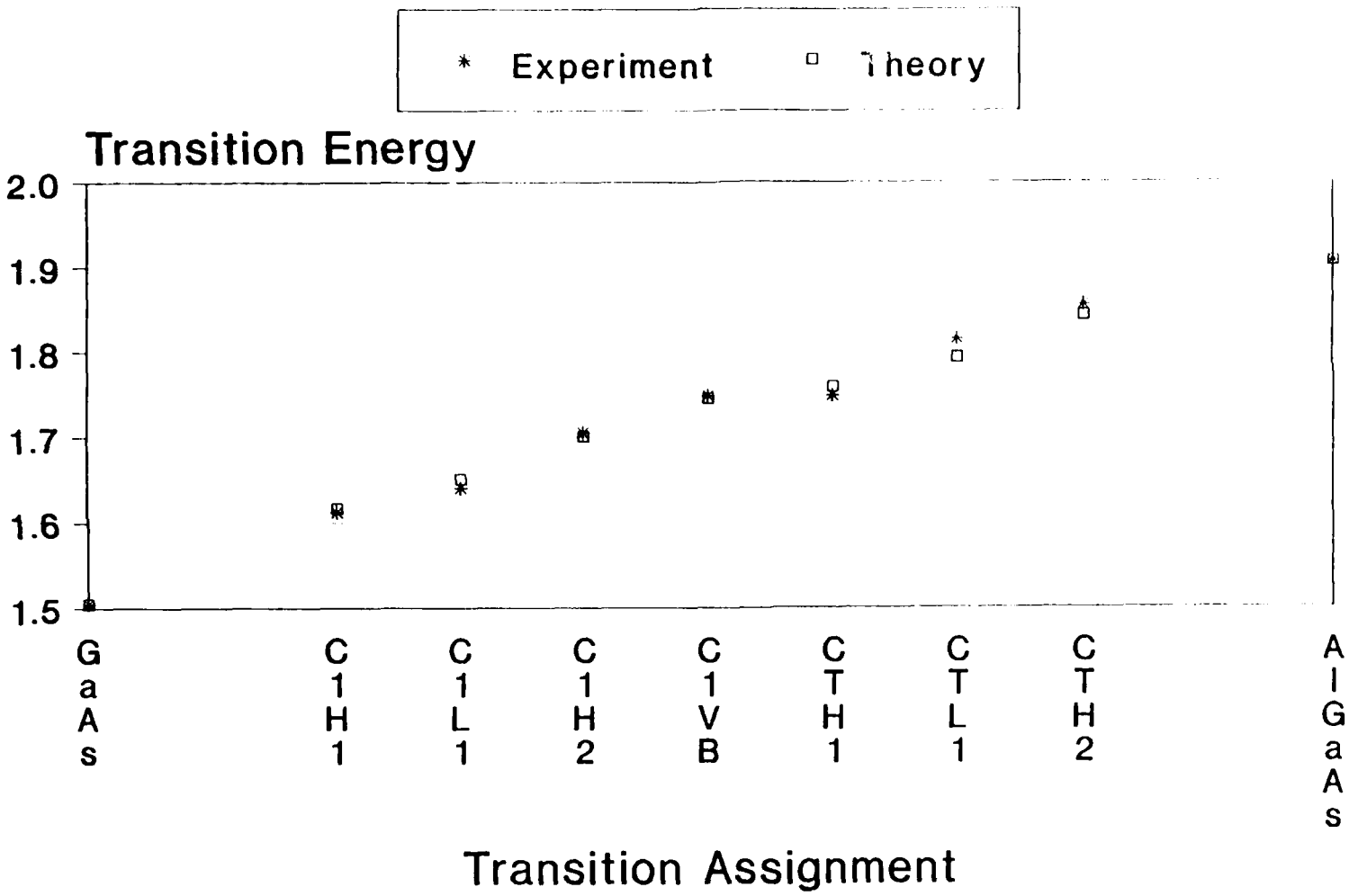

M. H. Herman, et al "Electron Beam Electroreflectance ..."
Figure 8

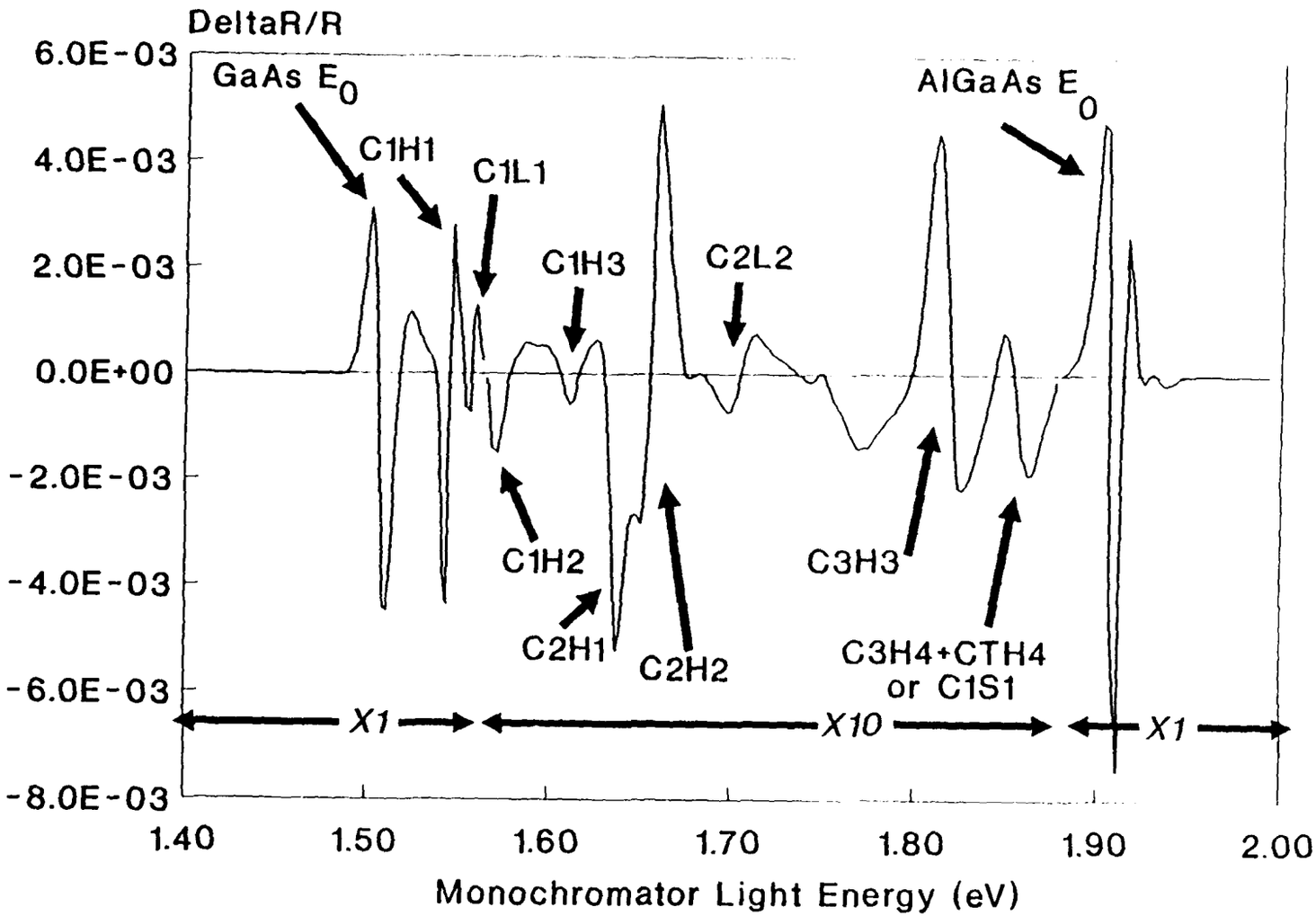

M. H. Herman, et al "Electron Beam Electroreflectance ..."
Figure 9

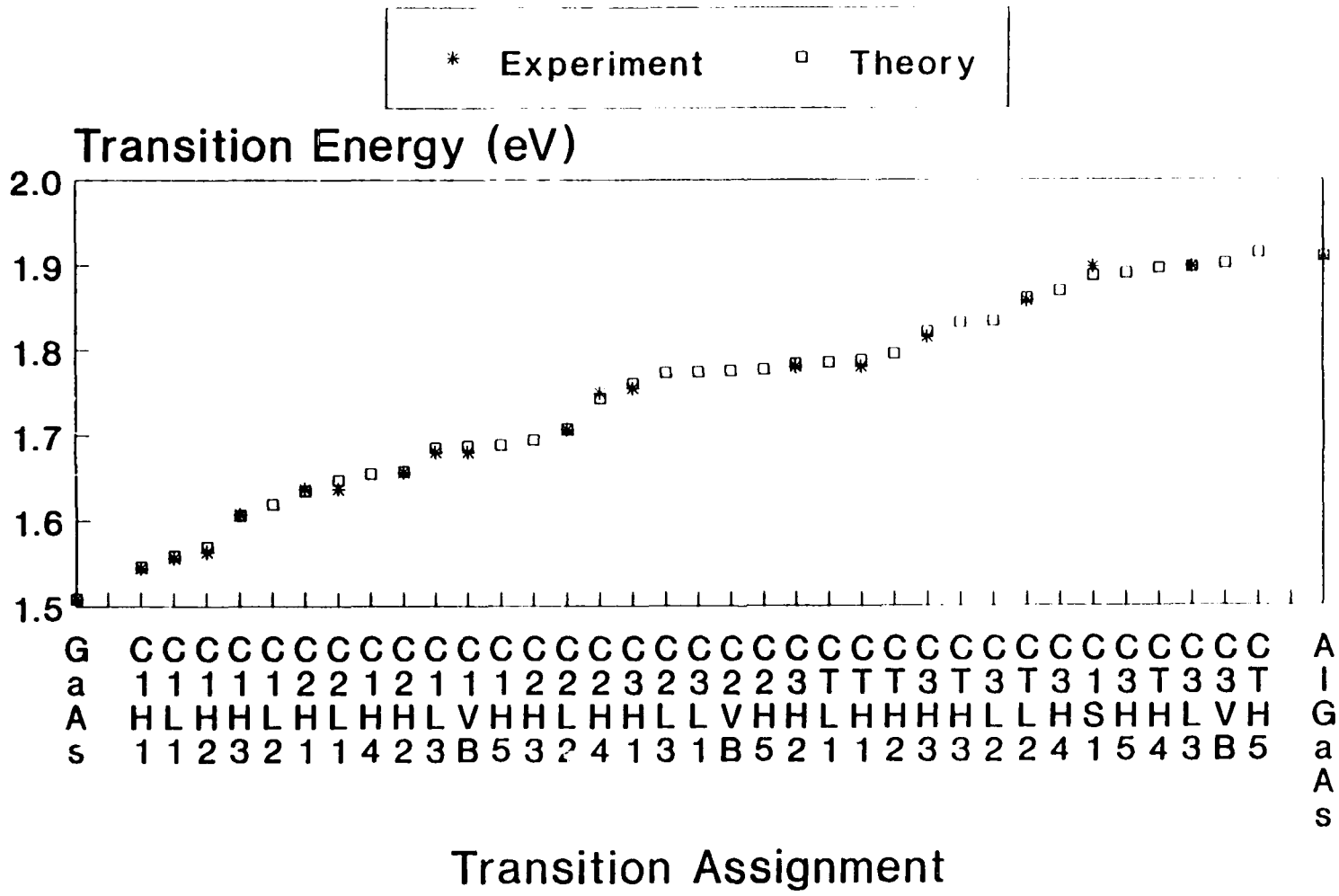

M. H. Herman, et al "Electron Beam Electroreflectance ..."
Figure 10